Lithos 364–365 (2020) 105535

Contents lists available at ScienceDirect

Lithos

journal homepage: www.elsevier.com/locate/lithos

Research Article

Mixing of heterogeneous, high-MgO, plume-derived magmas at the base of the crust in the Central Iapetus Magmatic Province (Ma 610-550): Origin of parental magmas to a global LIP event

Thomas B. Grant [a,*], Rune B. Larsen [a], Eric L. Brown [b], Axel B. Müller [c], Suzanne McEnroe [a]

[a] Department of Geoscience and Petreoleum, Norwegian University of Science and Technology Faculty of Engineering (NTNU), Trondheim 7491, Norway
[b] Aarhus University, Denmark
[c] Natural History Museum, Oslo, Norway

ARTICLE INFO

Article history:
Received 1 November 2019
Received in revised form 10 April 2020
Accepted 11 April 2020
Available online 15 April 2020

Keywords:
Ultramafic intrusion
Lower crust
Picrite magma
Recharge and fractional crystallisation
Inhomogeneous mantle plume

ABSTRACT

High-MgO (>12 wt%) magmas represent some of the most primary and high temperature melts from mantle plumes. The compositional diversity of high-MgO magmas gained by fractional melting within inhomogeneous mantle sources, is often overprinted by wall rock assimilation, magma mixing and fractional crystallisation within magma chambers at various depths within the crust. The deepest intrusions, at the base of the crust, are the first stop for magmas as they leave the mantle and such localities offer vital insights into the crustal processes that modify high-MgO melts. The Seiland Igneous Province (SIP) represents a rare exposure of a deep crustal magma conduit system that transported large volumes of mantle-derived melts through the lower continental crust. In this work, trace element compositions of clinopyroxenes in dunite, wehrlite and olivine clinopyroxenite samples from the Reinfjord intrusion were measured using laser-ablation inductively coupled plasma mass spectrometry (LA-ICP-MS). The melts calculated to be in equilibrium with the clinopyroxenes represent derivatives of mantle-derived magmas and have steep rare earth element (REE) profiles with La/Yb_{PM} of 8.4–14., Sm/Yb_{PM} of 3.5–4.8, and negative anomalies in Nd, Zr and Hf. Assimilation, recharge and fractional crystallisation modelling shows that the ultramafic cumulates in the Reinfjord intrusion formed through concurrent fractional crystallisation and repetitive recharge (and mixing) of new primitive magmas from the mantle with very limited input from crustal sources. The recharge and mixing model is strongly supported by field and petrographic data. Two end-member ultramafic magmas are identified; the first end-member melt composition ($MELT_{CPX0}$) is similar to the melt compositions that are in equilibrium with the most trace element depleted clinopyroxenes from Reinfjord. The second end-member melt composition ($MELT_{PIC0}$) is similar to a number of picrite dykes found throughout the SIP, which have less steep LREE/HREE and lack strong negative anomalies in Zr and Hf. The REEBOX PRO melting model (Brown and Lesher, 2016) was used to forward model adiabatic decompression melting of lithologically homogeneous and heterogeneous sources containing anhydrous/hydrous peridotite ± pyroxenite. It was found that $MELT_{PIC0}$ formed by melting of a peridotite source with up to 10% pyroxenite component and mantle potential temperatures of up to 1450 °C. $MELT_{CPX0}$, however, formed by melting of a carbonate- metasomatised peridotite with potential temperatures of up to 1630 °C. These results indicate a compositionally and thermally inhomogeneous mantle plume beneath the SIP.

1. Introduction

Large Igneous Provinces (LIPs) transfer huge volumes of magmas (>0.1 MKm^3) from the mantle into the crust, where they form intermittent magma chambers or are erupted as continental flood basalts (CFB), within short time spans of ~50Myr (Bryan and Ernst, 2008; Ernst, 2014). Most CFB, and the exposures of shallow intrusions in LIPs, have evolved compositions of <8 wt% MgO (Jennings et al., 2017; Sobolev et al., 2009) that indicate differentiation at deeper levels of the crust. Rarer, high-MgO (>12 wt%) magmas containing primary phenocrysts of highly forsteritic olivine (>Fo_{90}) are considered to be the purest records of the most primitive magmas generated in the mantle beneath LIPs (e.g. Heinonen et al., 2015; Jennings et al., 2017; Kamenetsky et al., 2012; Thompson and Gibson, 2000). High-MgO magmas are often divided into two groups; ferropicrites and picrites. Ferropicrites are thought to be derived from melting of mantle sources that contain a component of pyroxenite, and picrites are derived from melting of peridotite sources (e.g. Gibson, 2002; Jennings et al., 2017; Kamenetsky et al.,

* Corresponding author.
E-mail addresses: tomgrant.gfz.fu@googlemail.com (T.B. Grant), rune.larsen@ntnu.no (R.B. Larsen).

https://doi.org/10.1016/j.lithos.2020.105535

2012). The expression of clear groups of high-MgO magmas in several LIPs most likely originates from high temperature melting within a mixed mantle plume source that contains both pyroxenite and peridotite lithologies (Gibson, 2002; Kent et al., 2002).

The major and trace element chemistry of melt inclusions within primary olivine phenocrysts shows a wider range in compositions compared to their host magmas (Jennings et al., 2017; Kamenetsky et al., 2012; Kent et al., 2002; Nielsen et al., 2006; Yaxley et al., 2004; Yu et al., 2015). The chemical discrepancy of melt inclusions compared to their host magmas indicate that high-MgO magmas are affected by varying degrees of recharge, eruption, assimilation and fractional crystallisation processes (REAFC) within magma chambers at deeper levels of the crust (Jennings et al., 2017, Kamenetsky et al., 2012, Kent et al., 2002, Nielsen et al., 2006, Yaxley et al., 2004, Yu et al., 2015). Unfortunately, these deep-crustal magma chambers are rarely preserved in the geological record and prevent direct observations of the parental magmas producing the shallow LIP systems. The Reinfjord Ultramafic Complex (RUC), in the Seiland Igneous Province (SIP), is an ultramafic conduit system exposing a deep crustal cross-section (0.6–1 GPa) of a high yielding system through which large volumes of melt passed (Grant et al., 2016; Larsen et al., 2018). The RUC comprises the deepest exposed parts of the Ediacaran Central Iapetus Magmatic Province and according to most studies (e.g. Larsen et al., 2018; Tegner et al., 2019) formed at the impingement of a mantle plume under the Rodinian Supercontinent.

In the RUC, we obtain and discuss trace element compositions of clinopyroxenes measured in 9 samples (3 dunites, 4 wehrlites, and 2 olivine clinopyroxenites) using laser-ablation inductively coupled plasma mass spectrometry (LA-ICP-MS). The geochemical data are used to calculate the composition of the melts that formed the clinopyroxenes and to provide (semi-) quantitative constraints, along with petrographic and field data, on the relative importance of fractional crystallisation, wall-rock assimilation and magma mixing/recharge within the Reinfjord magma chamber. The results are then compared to the compositions of high-MgO magmas and olivine hosted melt inclusions from Emeishan (Kamenetsky et al., 2012), Paraná-Etendeka (Gibson, 2002; Jennings et al., 2017; Thompson and Gibson, 2000) and Karoo (Heinonen et al., 2015; Jennings et al., 2017; Riley et al., 2005) that are also thought to be fed by deep seated conduit systems. Forward models of adiabatic decompression melting of lithologically homogeneous and heterogeneous sources containing anhydrous/hydrous peridotite ± pyroxenite (using the REEBOX PRO melting model of Brown and Lesher, 2016) are used to determine the potential mantle sources of the ultramafic magmas in the SIP. Finally, we use our results to discuss the diversity of melts in the deep-seated parts of high yielding magmatic systems and the implications for the genesis of the Ediacaran Central Iapetus Magmatic Province.

2. The seiland igneous province

The Seiland Igneous Province (SIP) consists of large volumes (>17,000 km^3) of mafic, ultramafic, alkaline and felsic rocks (Larsen et al., 2018; Pastore et al., 2016) (Fig. 1.) that were intruded into Neoproterozoic metasediments (Corfu et al., 2007) at pressures corresponding to the lower crust (0.6–1 GPa – e.g. see estimates within Bennett et al., 1986; Grant et al., 2016; Griffin et al., 2013; Larsen et al., 2018; Sørensen et al., 2019; Tegner et al., 1999; Orvik, 2019). As the SIP only records the lower crustal section of the province, it is likely that the total volumes of magma are much larger than those currently exposed or inferred using gravimetric data (Larsen et al., 2018; Pastore et al., 2016). The results of 3D gravity modelling reveal that most of the SIP has a thickness of 2–4 km, with three deep ultramafic roots that extend 9 km below the present surface of Seiland, Stjernøy and Sørøy (Pastore et al., 2016). The thickness of the nappe structure indicates that the province has not undergone significant tectonic reworking during the Caledonian Orogeny (Pastore et al., 2016). Recent age data shows that the majority of the mafic, alkaline and felsic rocks in the SIP formed within a narrow time range between 580 and 560 Ma (Roberts et al., 2006; Roberts et al., 2010), with a later pulse of nepheline syenite pegmatites at 530–520 Ma (Pedersen et al., 1989; Roberts et al., 2010). The SIP is spatially and temporally linked to the Central Iapetus Magmatic Province, which stretched through Baltica and Laurentia, and includes numerous dyke swarms, intrusions and carbonatite complexes all with ages between 615 and 550 Ma (Ernst and Bell, 2010; Tegner et al., 2019). Isotopic signatures of alkaline, carbonatite, mafic and ultramafic intrusions in the SIP ($^{87}Sr/^{86}Sr$; 0.7038, ε_{Nd}; +4, and ε_{Hf}; +8) are similar to MORB and OIB compositions, suggesting a sub-lithospheric mantle source (Griffin et al., 2013; Mørk and Stabel, 1990; Roberts et al., 2010; Tegner et al., 1999). Estimates of the absolute temperatures of ultramafic magmas in the SIP vary between 1450 and 1650 °C, implying the involvement of an unusually hot mantle plume that may have originated at the core-mantle boundary (Bennett et al., 1986; Griffin et al., 2013; Robins and Gardner, 1975).

The SIP contains four large mafic-ultramafic complexes; Reinfjord (Emblin, 1985; Grant et al., 2016), Melkvann (Yeo, 1984), Kvalfjord (Svensen, 1990) and Nordre Brumandsfjord (Griffin et al., 2013) as well as numerous smaller hornblende-clinopyroxene rich intrusions. The ultramafic intrusions are the de facto main conduits through which large volumes of magmas passed (Larsen et al., 2018) (Fig. 1) and they are situated in a *right way up* position with parts of the roof section preserved in the highlands at 700–900 m above sea level. All four ultramafic intrusions were preceded by large layered mafic intrusions, which were directly emplaced into Neoproterozoic metasediments forming large amphibolite to granulite facies contact aureoles (Bennett et al., 1986; Tegner et al., 1999). In Reinfjord, Melkvann and Kvalfjord, the intrusive sequence was mafic (gabbro-gabbro-norite) - > ultramafic (dunite, pyroxenite, peridotite) - > picrite-ankaramite-lamprophyre dykes (Bennett et al., 1986; Larsen et al., 2018). The ultramafic complexes of Melkvann, Kvalford and Nordre Brumandsfjord are dominated by exposures of roof zones and marginal zones that are strongly contaminated by the wall-rock gabbros (Larsen et al., 2018). At Reinfjord, uncontaminated cumulate sequences in the core of the intrusion provide a truer record of the composition of cumulates formed by the most primary, ultramafic magmas in the SIP (Larsen et al., 2018). The composition of the ultramafic melts in Reinfjord, Melkvann and Kvalfjord are poorly constrained but are thought to be picrite-komatiite melts with MgO contents of 20–25 wt% MgO, absolute temperatures of up to 1450 °C and compositions similar to the late picrite-ankaramite dykes observed throughout the SIP (Bennett et al., 1986; Reginiussen et al., 1995; Robins, 1975; Robins and Takla, 1979; Yeo, 1984).

3. Field relationships of the Reinfjord ultramafic complex

The Reinfjord Ultramafic Complex (Fig. 1b) is emplaced into gabbro-norite and metasediment host rocks. Most of the intrusive contacts are between the ultramafic rocks and the surrounding gabbro-norite. In the south-west, ultramafic units intrude into both the gabbro-norite (above) and the metasediments (below). The intrusion is concentrically zoned with a core of cryptically layered dunite and wehrlite (Central Series), rhythmically and modally layered olivine clinopyroxenites and wehrlites in the middle (Upper Layered Series), and a large layered gabbro-norite envelope that surrounds the ultramafic units.

3.1. The upper layered series (ULS)

The ULS is exposed to the east of the CS on a plateau region between 500 and 900 m above sea level and to the west of the CS in steep cliffs. The ULS is a rhythmically and modally layered sequence with at least 7 cyclic units and over 250 m of cumulate stratigraphy (Emblin, 1985). The base of each unit is composed of olivine dominated cumulates of dunite and poikilitic wehrlite (Fig. 2C), whereas the upper

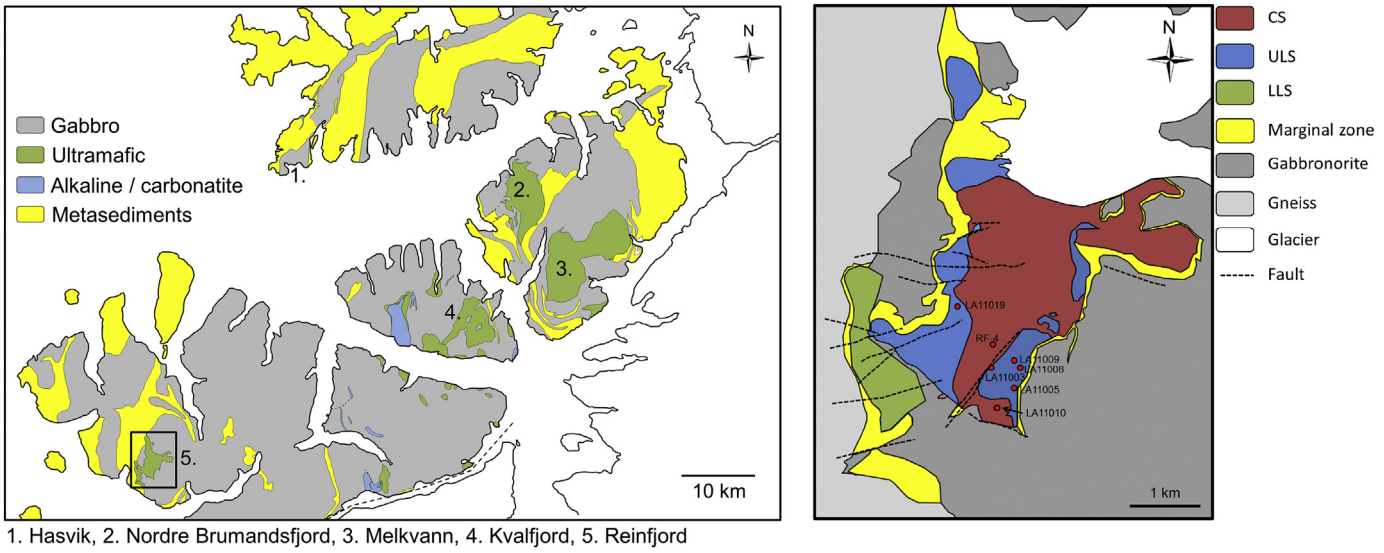

Fig. 1. (a) Simplified regional map of the Seiland Igneous Province modified from maps of Bennett et al. (1986), Griffin et al. (2013) and Tegner et al. (1999) with the new regional map of Reinfjord from Grant et al. (2016). (b) Geological map of the Reinfjord Ultramafic complex modified from Grant et al. (2016). Central series (CS), upper layered series (ULS) and lower layered series (LLS).

sections of each unit are composed of olivine and clinopyroxene dominated cumulates of wehrlite and olivine clinopyroxenite. The thickness of the units ranges from around 10 m to over 100 m (Emblin, 1985) but individual modal layers have thicknesses from several centimeters to several meters (Fig. 2A and Fig. 2C). Excellent field exposures of slumping, cross-bedding, load-structures, ball and flame structures and even recharge events of fresh melts are observed in the ULS (Larsen et al., 2018). The ULS is separated from the gabbro-norite host rocks by <150 m wide marginal zones.

3.2. The central series (CS)

The CS occupies the central parts of the intrusion and is exposed on a plateau region from 600 to over 900 m above sea level. Drill cores reveal that the CS extends down to 400 m below the plateau meaning that more than 700 m of cumulate stratigraphy is accessible. The CS predominantly consists of dunite and poikilitic wehrlite with no modal layering but variations in bulk rock chemistry and olivine compositions show clear evidence of cryptic layering (Emblin, 1985; Grant et al., 2016; Larsen et al., 2018). Changes in olivine composition from forsterite 79 to 85 over 1–2 m indicate that the boundary between units can be relatively sharp and that reversals in mineral compositions indicate recharge of new magma (Grant et al., 2016). Irregular replacive dunites are observed at the contacts between the CS and the ULS (Fig. 2B and Fig. 2D) and crosscut the layering of the ULS discordantly. Replacive dunites are observed as meter-scale dykes, irregular centimetre- to meter-scale protrusions in the layering of the ULS and at micron- to centimetre-scales as interstitial channels of olivine grains within some olivine clinopyroxenite samples from the ULS (Grant et al., 2016). The field and petrographic observations of replacive dunites strongly suggest CS-forming magmas intruded into the ULS cumulates whilst they were in an unconsolidated state and the timing between the formation of the two series was short. The field data and drill core sections indicate very limited lateral variation in the CS cumulates in terms of modal mineralogy and bulk rock compositions (Larsen et al., 2018). The CS cumulates are post-dated by numerous dykes of wehrlite, olivine clinopyroxenite, hornblende clinopyroxenite, gabbro and alkaline dykes of alkali basalt, alkaline gabbro and lamprophyre compositions (Grant et al., 2016; Larsen et al., 2018; Orvik, 2019). The central series intrudes into gabbro wall-rocks to the north- and north-east, forming similar marginal zones to those between the ULS and gabbro.

3.3. Marginal and roof zones

The marginal zones are hybrid zones consisting of un-layered coarse-grained websterites, recrystallised gabbro-norite xenoliths, anorthosites and plagioclase-bearing peridotite. Plagioclase is absent in the ULS and CS cumulates and only appears within the marginal zones. Both the gabbro-norite xenoliths within the marginal zones and the wall-rock gabbro-norite (for up to 50–100 m away from the ULS contacts) are strongly deformed and contain recrystallised leucogabbro. Anorthositic xenoliths are the residua of partial melting of gabbro-norite as pyroxene is progressively lost (Bennett et al., 1986; Grant et al., 2016; Griffin et al., 2013; Larsen et al., 2018). Partial melts extracted from the gabbro contaminate the incoming ultramafic melts forming plagioclase-bearing peridotites and coarse-grained websterites (Bennett et al., 1986; Emblin, 1985;Grant et al., 2016; Larsen et al., 2018). Recrystallised gabbro-norite xenoliths range in size from several centimeters to over 100 m (Fig. 2E) and lie subparallel to the layering in the ULS. The degree to which the marginal zones are contaminated by partial melting of the gabbro-norite is evident in the bulk rock geochemistry with linear mixing trends in major elements between the ULS or CS and the gabbro-norites (Grant et al., 2016; Larsen et al., 2018). The majority of the ULS and CS do not display the geochemical, field or petrographic evidence of contamination that are so clearly recorded in the marginal zones.

4. Petrography

A total of 9 samples were studied. The samples include 4 from the CS and 5 from the ULS, together they are comprising 3 dunites, 4 wehrlites, and 2 olivine clinopyroxenites (see Table 1.). The locations of the samples are shown in Fig. 1b. Three samples from the CS are from drill cores RF-4 and are located on the map under the point RF-4. The number system for the drill core samples includes the drill core number and the depth in meters in the drill core. For example, sample RF4–274.8 is from 274.8 m depth in drill core RF-4. The samples are unaltered except for a few thin serpentinite veins. Bulk rock compositions are reported in Table 1. Accessory amounts of interstitial magmatic chromian-spinel,

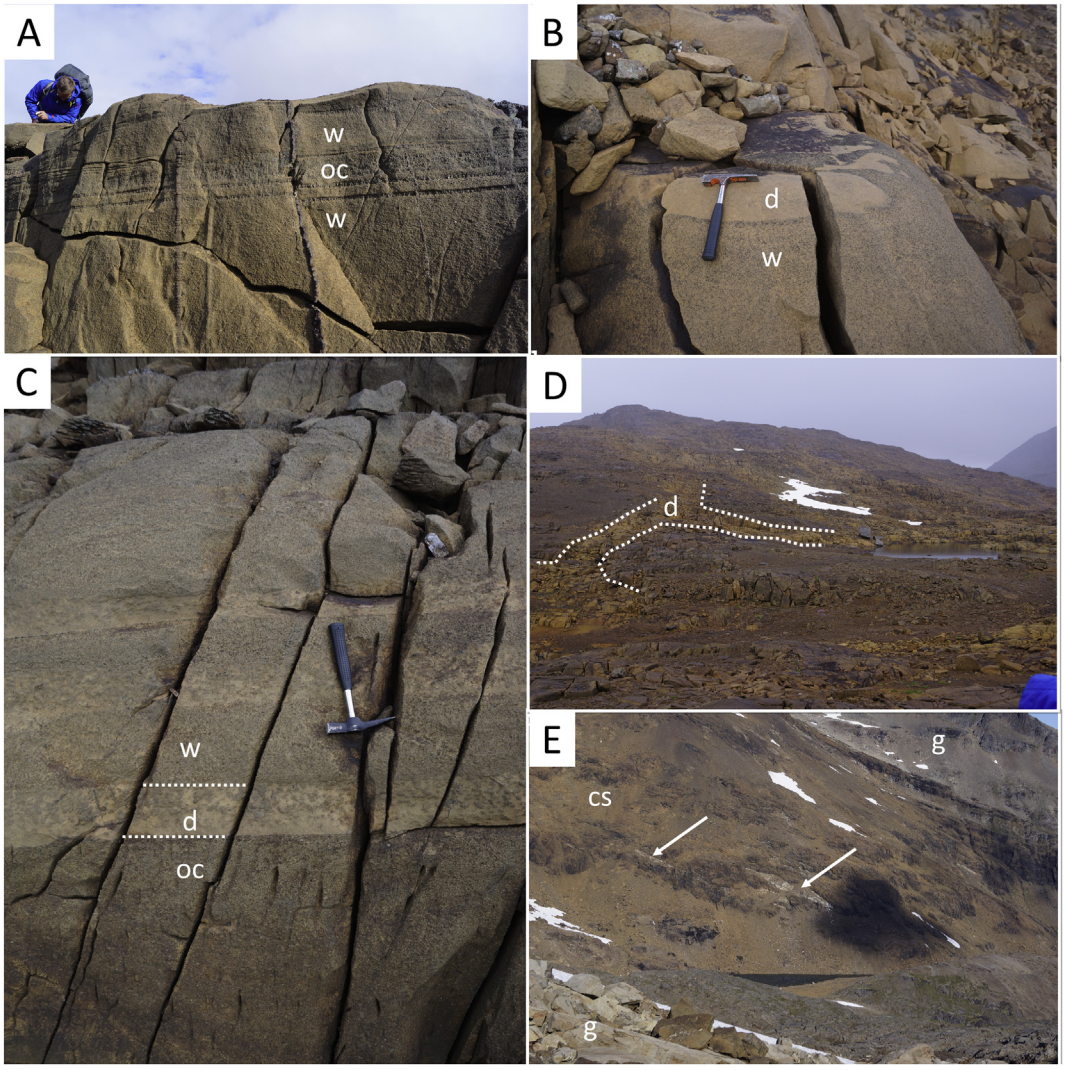

Fig. 2. w – wehrlite, d – dunite, oc – olivine clinopyroxenite, g – gabbro, cs – central series, white dotted lines are examples of contacts between rock types i.e. layering or intrusive contacts, white arrows highlight gabbro xenoliths. **A** – Layering in dunite-wehrlite. Thick units (up to 2 m) with thin layers of olivine clinopyroxenite (2–40 cm) in the western ULS section. **B** – Wehrlite disturbed by irregular replacive dunite. A flow direction from left to right (West to East) appears to be likely. The image was taken in the Western section of the ULS, close to the border between the CS and ULS. **C**. A thick olivine clinopyroxenite layer is overlain by thinner, repeating sequences of dunite - wehrlite in the western ULS. **D**. Replacive dunite dykes of meter-scale interconnecting in the south-west facing slope of the western ULS. The CS is 50–100 to the east of the image. **E**. Large 100 m scale xenoliths of metagabbro in the NW ULS. The xenoliths are orientated sub-parallel to the layering of the ULS and the host gabbro. Note that the gabbro to the right of the image (NE) is above the ULS and rises to the NW (towards the top left of the image) to a roof zone. In the foreground, the eastern ULS-Gabbro contact is visible as light grey marginal zone metagabbros.

sulfides (pentlandite, pyrrhotite and chalcopyrite) and carbonates (dolomite, magnesite) are common in dunite, wehrlite and olivine clinopyroxenite samples but are not discussed in detail here.

Dunite samples contain >90% olivine. The olivines are mostly coarse-grained (up to 0.5–2 cm), irregularly shaped cumulus olivine grains that are internally deformed (kink banding) (see Fig. 3A) (Grant et al., 2016). Smaller, interstitial olivines with low degrees of internal deformation, and euhedral to subhedral shapes may have formed through the crystallisation of olivine saturated interstitial melt (Grant et al., 2016) or by deformation and recrystallisation (Sørensen et al., 2019). Larger olivines contain inclusions of euhedral Fe-Cr-rich spinel, rods of ilmenite and/or magnetite and trails of dolomite + magnetite + enstatite ± fluid. The inclusion trails record a similar reaction to shear zones of olivine + clinopyroxene + CO_2 = enstatite + dolomite, which formed at 750–850 °C and c. 1 GPa pressures (Larsen et al., 2018; Sørensen et al., 2019). Clinopyroxene appears mostly as highly irregular shaped interstitial grains along olivine grain boundaries (Fig. 3B, LA11010, RF4–224.3) or as larger oikocrysts. In some samples clinopyroxenes are observed as large (up to 5 cm) pegmatitic grains (e.g. sample RF4-274.8). Clinopyroxenes in all samples contain exsolution lamellae of orthopyroxene, Cr-Al-spinel and magnetite. Intercumulus orthopyroxene is rare but some orthopyroxene is observed as thin rims between interstitial clinopyroxene and olivine.

Wehrlites contain between 10 and 50% clinopyroxene. Samples from Reinfjord span this entire range in modal mineralogy and this is reflected in the bulk rock chemistry (Emblin, 1985; Grant et al., 2016). Olivine textures are similar to those in dunites. In samples with higher olivine contents, olivine is predominantly a cumulus phase and clinopyroxene mostly occurs as large ovoid clinopyroxene oikocrysts enclosing olivine chadocrysts (e.g. sample LA11009 and LA11019, Fig. 3C). With increasing clinopyroxene content, cumulus clinopyroxene with grain sizes of 1–4 mm becomes more common and poikilitic clinopyroxene becomes less common. This can be observed in the differences between sample LA11019 in Fig. 3B and C compared to sample LA11003 in Fig. 3D.

Olivine clinopyroxenites (LA11005 and LA11008) contain over 50% clinopyroxene and consist of large (1–3 mm) cumulus clinopyroxene and olivine (Fig. 3E–F). Some samples have proportions of

Table 1
Bulk rock compositions from Grant et al. (2016). Rock types; D = dunite, W = wehrlite, OC = olivine clinopyroxenite. Samples from the drill core RF4 are noted with the depth at which the sample was taken from in meters, e.g. RF4-274.8 was taken at 274.8 m depth. – denotes a measurement that is below the detection limits. Major element analyses were made using X-ray fluorescence (XRF) and trace elements by inductively coupled plasma mass spectrometry (ICP-MS) as ALS-Chemex Malå, Sweden (for further details of standards and duplicate analyses see Grant et al., 2016).

Sample	RF4-274.8	RF4-298.1	RF4-224.3	LA11010	LA11003	LA11009	LA11019	LA11005	LA11008
Unit	CS	CS	CS	CS	ULS	ULS	ULS	ULS	ULS
Rock type	D	D	W	D	W	W	W	OC	OC
SiO_2	38.8	37.4	38.5	38.2	44.0	41.6	39.7	47.7	44.2
TiO_2	0.1	0.1	0.1	0.3	0.3	0.2	0.1	0.9	0.4
Cr_2O_3	0.4	0.5	0.1	0.5	0.4	0.3	0.1	0.3	0.4
Al_2O_3	0.3	0.5	0.4	0.9	1.3	0.9	0.6	3.6	1.8
Fe_2O_3	15.9	16.4	15.7	19.8	11.0	13.9	17.4	10.8	12.1
MnO	0.2	0.2	0.2	0.2	0.2	0.2	0.2	0.2	0.2
MgO	42.3	42.1	41.4	40.8	34.2	38.5	35.8	19.4	31.3
CaO	0.8	0.9	1.7	1.0	8.1	3.9	2.9	14.8	8.4
Na_2O	–	–	–	–	0.2	0.1	–	0.4	0.2
K_2O	–	–	–	–	–	–	–	–	–
P_2O_5	–	–	–		–	–	–	0.1	0.1
Total	98.8	98.0	98.0	101.6	99.7	99.5	96.9	98.1	99.1
Nb	–	–	–	0.2	0.3	0.2	1.1	0.4	0.3
La	–	–	–	0.5	0.6	0.5	0.5	1.3	0.8
Ce	–	0.6	–	0.7	2	1.4	1.2	5	2.6
Pr	0.04	0.06	0.09	0.1	0.41	0.25	0.20	1.04	0.49
Sr	1.7	3.6	3.4	4.6	20.8	10.2	8.6	39.2	22.3
Nd	0.3	0.4	0.4	0.5	2.2	1.3	1	6	2.7
Zr	–	3	2	3	7	5	3	22	10
Hf	–	–	–	0.2	0.3	0.2	0.2	1.0	0.4
Sm	0.05	0.10	0.15	0.17	0.72	0.44	0.32	2.08	0.91
Eu	0.03	0.06	–	0.06	0.27	0.15	0.10	0.75	0.34
Gd	0.07	0.20	0.18	0.20	0.88	0.52	0.36	2.66	1.21
Tb	0.02	0.04	0.03	0.03	0.13	0.07	0.05	0.39	0.18
Dy	0.13	0.18	0.18	0.21	0.77	0.45	0.34	2.43	1.02
Ho	0.02	0.03	0.03	0.04	0.14	0.09	0.06	0.45	0.19
Er	0.07	0.04	0.09	0.12	0.38	0.22	0.16	1.13	0.53
Tm	0.02	–	0.02	0.02	0.04	0.03	0.02	0.14	0.06
Yb	0.05	0.06	0.08	0.16	0.29	0.19	0.13	0.94	0.4
Lu	0.01	0.01	0.01	0.02	0.04	0.02	0.02	0.13	0.05
Y	0.6	0.6	0.7	1.0	3.5	2.1	1.6	10.7	4.6
Sc	6	6	8	–	–	–	–	–	–
V	17	27	24	62	57	55	109	266	107
Cr	2460	3570	690	3770	2970	2060	870	2510	2800
Co	153	149	140	171	109	151	166	87	125
Zn	100	109	107	139	65	83	115	57	69

approximately 80–85% clinopyroxene and 15–20% olivine (approximate cotectic proportions). However, olivine clinopyroxenites show a continuum between 50 and 85% clinopyroxene and this is also reflected in the bulk rock compositions (Grant et al., 2016). Samples with non-cotectic proportions contain interstitial networks of smaller olivine and clinopyroxene grains between the larger cumulus olivine and clinopyroxene grains (Fig. 3E and F). Interstitial amphibole in sample LA11005 is closely associated with clots of dolomite + plagioclase + biotite that show reactive and replacement textures against the surrounding clinopyroxene and olivine.

4.1. Crystallisation sequence

The first phases to crystallise are olivine ± spinel. Variations of Mn concentrations in olivine from the CS (0.16–0.24 wt%) with partition coefficients of 0.85–0.9 (Kohn and Schofield, 1994) indicate up to 15–20% fractional crystallisation prior to clinopyroxene, consistent with experimental crystallisation data on picrites (Müntener and Ulmer, 2006; Tuff et al., 2005). Olivine is followed by clinopyroxene, which always appears before plagioclase, except for in the contaminated marginal zones. Olivine clinopyroxenites with olivine: clinopyroxene ratios of 15:85 are consistent with crystallisation along the olivine and clinopyroxene cotectic (Grant et al., 2016; Presnall et al., 1978). Amphibole crystallises either before plagioclase or along with plagioclase in interstitial clots. The crystallisation sequence in the ultramafic rocks in Reinfjord is olivine ± spinel → olivine + clinopyroxene → clinopyroxene + amphibole ± plagioclase (Emblin, 1985; Grant et al., 2016) and is similar to the Kvalfjord (Svensen, 1990) and Melkvann ultramafic complexes (Yeo, 1984) as well as experimental studies on wet picrite melts at 1 GPa (Müntener and Ulmer, 2006).

5. Analytical methods

5.1. Electron probe micro-analysis (EPMA)

All EPMA analyses were conducted at the Norwegian University of Science and Technology (NTNU), Trondheim, using a JEOL JXA-8500F thermal field emission electron probe micro-analyser (EPMA). For all silicate analyses, EPMA conditions of 15 KeV and 20 nA were used. Natural samples were used for standards. Counting times for Na and K were 10 s on peak, Mg, Ca and Fe had 20 s on peak and Al, Si, Ti, Cr, and Mn had 30 s on peak. All elements had detection limits of approximately 200 ppm, except for Na that had 400 ppm. The large volume of ablated material from the LA-ICP-MS will include the exsolutions of spinel and magnetite within clinopyroxene. It was therefore necessary to obtain bulk (clinopyroxene + exsolutions) EPMA data for the clinopyroxenes. The most effective method of doing this is by using wide beam (20 μm) analyses (e.g. Berly et al., 2006). Comparisons between average wide beam and narrow beam (1 μm) analyses for each sample showed that SiO_2 did not change by more than 0.5 wt%, and in one case by only 0.01 wt%. Nevertheless, EPMA analyses using wide beams were used for the calibration of LA-ICP-MS data.

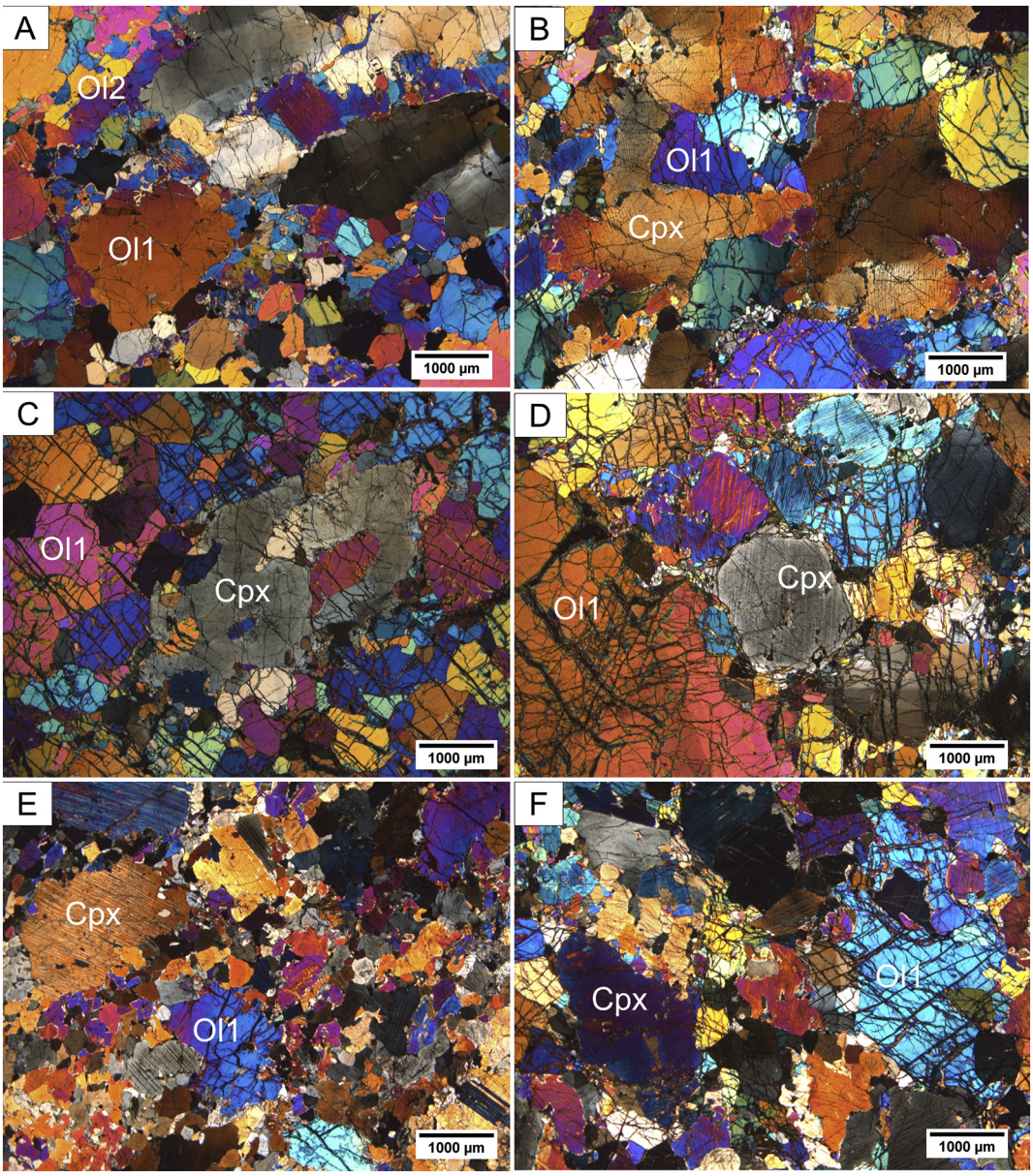

Fig. 3. Optical microscopy of samples. A – Sample LA11010 is a dunite with coarse, irregularly shaped olivine grains surrounded by smaller, subhedral to euhedral olivine. B – Sample LA11019 is a wehrlite with interstitial clinopyroxene around olivine grain boundaries. C – Sample LA11009 is a wehrlite with poikilitic clinopyroxene and olivine chadocrysts. D – Sample LA11003 is a wehrlite with cumulus clinopyroxene and large cumulus olivine. E – Sample LA11005 is an olivine clinopyroxenite with cumulus olivine and clinopyroxene with reaction textures against finer-grained intercumulus olivine and clinopyroxene. F – Sample LA11008 is an olivine clinopyroxenite with similar textures to sample LA11005.

5.2. Laser-ablation inductively coupled plasma mass spectrometry (LA-ICP-MS)

Rare earth elements (REE), Nb, Ti, Zr, Y, V, Cr, Co, Zn, Sc, Hf and Sr were measured in clinopyroxene, olivine from surface-polished thick sections (250–300 μm) using LA-ICP-MS at the Geological Survey of Norway, Trondheim (see supplementary materials for conditions). The ICP-MS used is a double focusing sector field inductively coupled plasma mass spectrometer (model ELEMENT XR from Thermo Scientific) linked to an excimer laser probe New Wave UP193FX ESI. The 193 nm laser had a repetition rate of 20 Hz, a spot size of 75 μm and an energy fluence of 5.5 to 6.5 J/cm^2 on the surface of the sample. The raster ablation area was approximately 500 × 150 μm. The ablated material was transported to the ICP-MS in a mixed He—Ar carrier gas. The Si^{29} isotope was used as an internal standard. The Si concentrations of clinopyroxene and olivine were measured prior to LA-ICP-MS by EPMA. A total of 29 LA-ICP-MS points on clinopyroxene used Si from EPMA points at the exact same location for both analytical techniques. A further 26 LA-ICP-MS points used Si from average SiO_2 concentrations for each of the samples from Grant et al. (2016). Four silicate glass reference materials (NIST SRM 610, NIST SRM 612, NIST SRM 614, NIST SRM 616, NIST SRM 1830) produced by the National Institute of Standards and Technology and a high purity silica glass (BCS 313) from the Bureau of Analysed Samples, UK, were used for external multi-standard calibration. Certified values for these reference materials were taken from Jochum et al. (2011) and Flem and Bédard (2002).

All measurements consisted of 15 scans of each element, with a measurement time of 0.0025 s per scan in the low (REE, Y, Zr, Sr, Hf, Nb) and medium mass resolution modes (Sc, Ti, V, Cr, Co, Zn). An Ar-blank was run before every sample and standard measurement to determine the background signal. In order to avoid memory effects between samples, the background signal was subtracted from the

instrumental response of the standard before normalization against the internal standard. A weighted least squares regression model using several measurements of all different standards was used to calculate the calibration curve for each element. The limits of detection (LOD) are based upon 3× standard deviation (3σ) of 10 NIST SRM 616 measurements. Two sets of analyses were taken. In each set there was a trade-off between the number of elements analysed and the time of each analysis to maximise the number of analyses taken within the available lab time at NGU. The first set included the elements Nb, Zr, Hf, Y, La, Ce, Nd, Sm, Eu, Gd, Tb, Dy, Ho, Er, Tm, Yb, Lu to investigate all REE. The second set included Sr, Zr, Hf, Y, La, Ce, Nd, Sm, Eu, Gd, Dy, Yb, Lu, Sc, Ti, V, Cr, Co, Zn to investigate a reduced number of REE with the addition of key transition metals and Sr.

6. Results

6.1. Clinopyroxene compositions

6.1.1. Major element compositions

All clinopyroxenes in the CS and ULS are mostly diopsidic and subsidiary augite in composition (supplementary materials). Clinopyroxenes have xMg ($Mg/(Mg + Fe^{2+})$) of 0.91–0.95 in dunites, 0.92–0.95 in wehrlites, and 0.88–0.94 in olivine clinopyroxenites. The major element compositions are very similar to those already reported for Reinfjord in Grant et al. (2016), who showed that the clinopyroxenes have increasing TiO_2 with Al_2O_3, which indicates fractionation without plagioclase. Core to rim variations in major elements show both normal and reverse zoning patterns within single clinopyroxene grains and this indicates that chemical trends during their crystallisation have been preserved during cooling (Grant et al., 2016).

6.1.2. Trace element compositions

The average clinopyroxene compositions for each sample and rock type show broadly similar trace element patterns: a small enrichment in trace elements (< factor of 3) relative to primitive mantle (Sun and McDonough, 1989) (Fig. 4) and a convex-downwards pattern with a small enrichment in LREE over HREE (La/Yb_{PM} of 2.05–1.61) and moderate enrichment of MREE over HREE (Sm/Yb_{PM} of 2.49–3.09). Negative anomalies are observed in Nb, Sr, Zr and Hf with only some samples showing small negative anomalies in Ti. The trace element patterns in clinopyroxene from Reinfjord are similar to those from average clinopyroxene in peridotites from Nordre Brumandsfjord (Griffin et al., 2013), except that the latter have higher trace element concentrations and have a more pronounced negative anomaly in Sr.

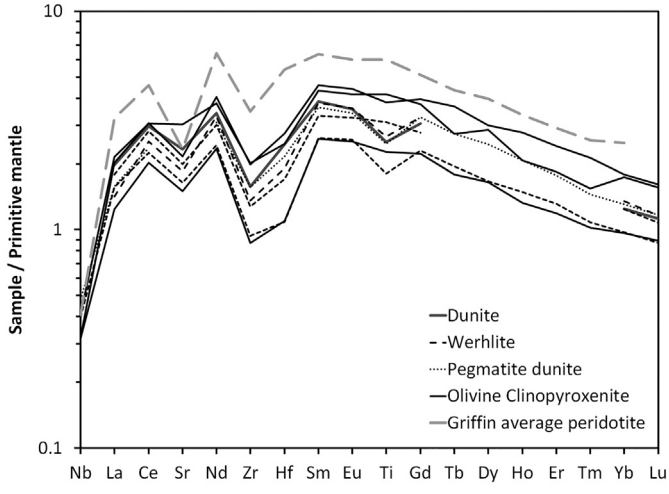

Fig. 4. Primitive mantle (Sun and McDonough, 1989) normalised clinopyroxene compositions.

All REE show positive correlations with Ti and the correlations are stronger for HREE compared to LREE (Fig. 5). The compositions of clinopyroxenes from wehrlites and dunites overlap but the most Ti and REE poor clinopyroxenes are from wehrlite. The greater range in trace element compositions in clinopyroxenes from wehrlites compared to dunites is most likely related to a sample bias due to the limited number of clinopyroxenes in dunite that were large enough to analyse. Major element concentrations from a much larger sample set from Grant et al. (2016) demonstrate that clinopyroxenes from dunites and wehrlites overlap in their compositions. Clinopyroxenes from olivine clinopyroxenites tend to have higher Ti and REE concentrations than those from wehrlites and dunites. Scandium and V also show positive correlations with Ti whereas Co and Zn show no clear correlation with Ti.

6.1.3. Core to rim variations

Detailed comparisons between core and rim compositions were not possible due to the large volume of material analysed in each point relative to the size of the clinopyroxene grains as well as the availability of large areas that were not fractured or altered by thin serpentinite veins. However, general statements can be made from comparisons between grains for a given sample. Core and rim analyses for samples LA11003, LA11008 and LA11009 are shown in Fig. 6. For sample LA11008, the analyses of clinopyroxene cores show a large range in trace element compositions but the rims of clinopyroxene have higher trace element concentrations than the cores. For sample LA11003, the core and rim compositions overlap but the highest measured trace elements were within a core. A core and rim comparison for a single grain shows that the core (LA11003–06-C) is slightly more trace element enriched than the rim (LA11003–06-B) with 11.01 ppm Zr and 9.75 ppm Zr respectively. For sample LA11009, the cores show a large variation in trace element abundances and are richer in trace elements than the two rim analyses from the same sample. Normal zoning is observed in a single grain from LA11019 with a trace element poorer core (e.g. 16.18 ppm Zr) and a trace element richer rim (e.g. 20.56 ppm Zr). A single grain in sample LA11005 is reverse zoned with higher trace element abundances in the core (e.g. 15.69 ppm Zr) lower trace element abundances in the rim (e.g. 12.88 ppm Zr). The compositional zoning patterns suggest that both normal zoning and reverse zoning patterns are present in the clinopyroxenes.

6.2. Olivine compositions

Olivines in the ULS vary from $Fo_{85.1}$ – $Fo_{77.4}$ whereas olivines from the CS vary from $Fo_{84.6}$ to $Fo_{76.1}$ (Grant et al., 2016). Our analyses show that the olivines contain very low abundances of all trace elements (Supplementary materials), which are mostly below the detection limits of the LA-ICP-MS. Olivines have Ti contents of <40 ppm and relatively homogenous amounts of Co across all samples of 160–190 ppm. Positive correlations between Y, Zr, Nd and Cr are observed. Due to the trace element concentrations being very low in olivine and small, local variations in the abundance of inclusions or any other secondary metasomatism and alteration dramatically affects their compositions. Olivine analyses are therefore not used for geochemically fingerprinting magma chamber processes in Reinfjord and are not discussed in further detail here.

7. Discussion

7.1. Parental melt compositions

Calculating the parental melt compositions from cumulate intrusive rocks is notoriously difficult. Trace element modelling methods such as those developed by Bédard (1994), Bédard (2001) may be invalid for rocks that have experienced complex processes of magma mixing or crustal contamination, which are recorded in the field data for the

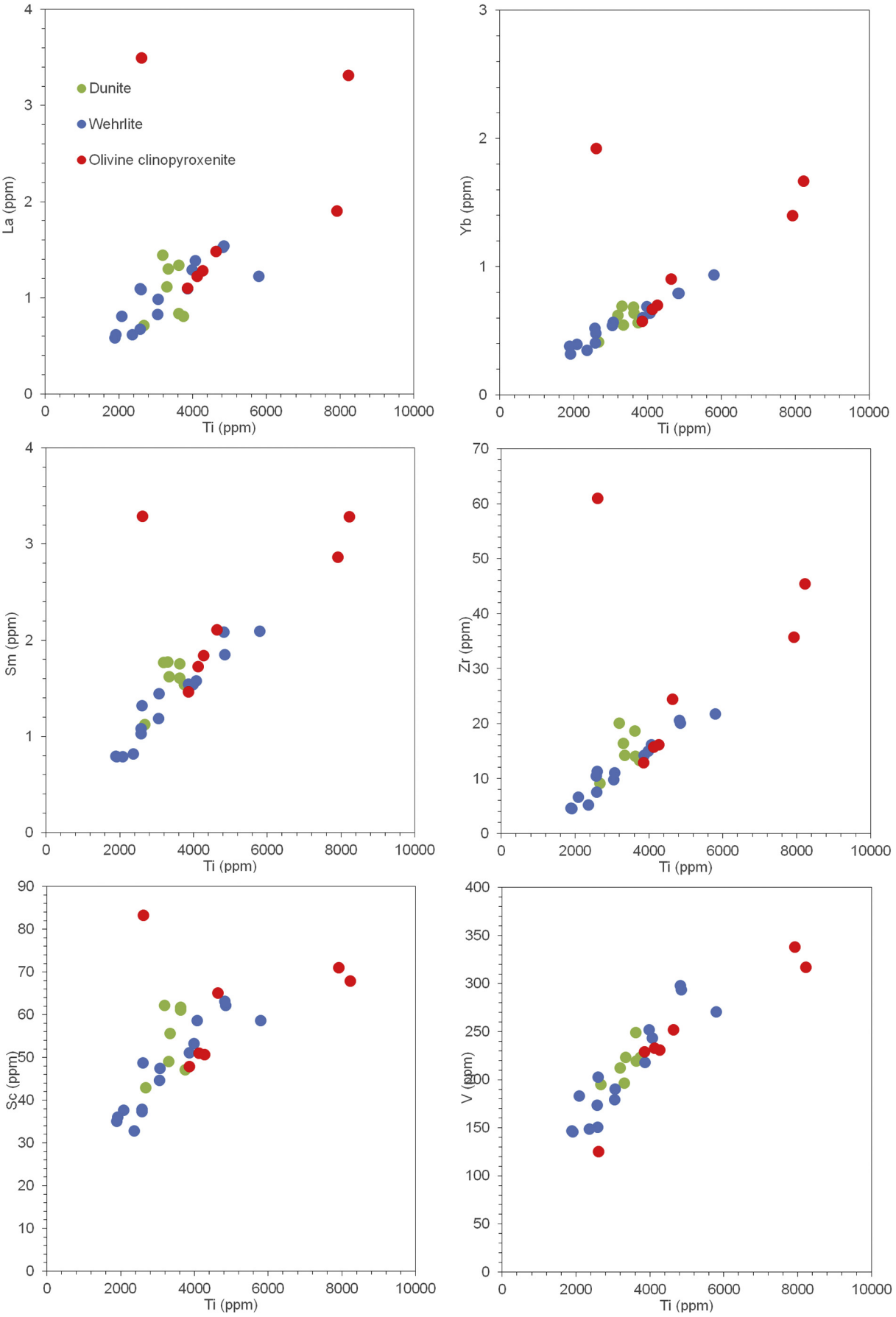

Fig. 5. Compositional variation of clinopyroxenes in wehrlite, olivine clinopyroxenite and dunite.

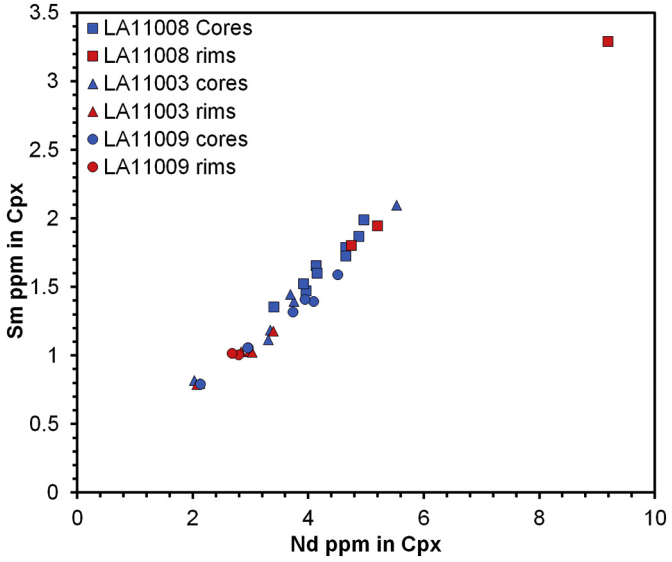

Fig. 6. Comparison between rim and core compositions of clinopyroxenes from samples LA11008, LA11003 and LA11009.

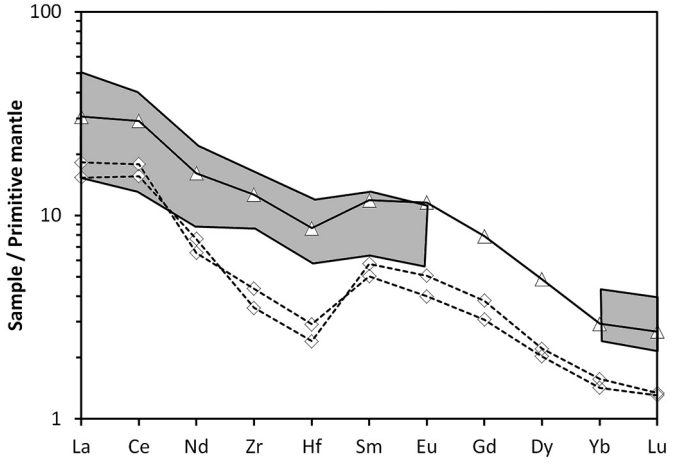

Fig. 7. Primitive mantle (Sun and McDonough, 1989) normalised melt compositions calculated from clinopyroxene compositions and partition coefficients from Bédard (2014). Grey field is the range of primitive mantle normalised compositions of picrite dykes from the SIP (Reginiussen et al., 1995; Robins, 1975; Robins and Takla, 1979; Yeo, 1984;), solid line with triangle symbols is the average of 14 calculated melt compositions, two dashed lines with diamond symbols are two of the most depleted melt compositions calculated.

cumulates from Reinfjord (Grant et al., 2016; Larsen et al., 2018). Core to rim variations in clinopyroxene indicate that each grain formed over changing melt compositions that may be related to fractionation, mixing or contamination. We therefore use a method that calculates the equilibrium melt composition for each clinopyroxene point analysis by calculating partition coefficients ($D_i^{Cpx/melt}$) from the parameterizations of Bédard (2014) and the relationships between the major element chemistry of the clinopyroxenes obtained by EPMA. For details of the method and the calculated melt compositions see Appendix 1. Our main assumption is that the trace element compositions of clinopyroxenes have not diffusively re-equilibrated with neighbouring mineral phases or internally re-equilibrated to homogenous grain-scale compositions during slow cooling of the intrusion. Variations in clinopyroxene compositions within single grains and within single samples indicate that this is a fair assumption to make in our samples. The calculated compositions track the melt evolution along the olivine + clinopyroxene cotectic as clinopyroxene crystallises. If we assume that the olivine compositions from the CS dunites record the amount of olivine that crystallised before reaching the olivine + clinopyroxene cotectic (10–15% Grannes, 2016), the melt compositions prior to olivine fractionation can be back calculated by using $D_i^{ol/melt}$ from Bédard (2005) and addition of 10–15% olivine (see supplementary materials 2).

The calculated melt compositions are enriched relative to primitive mantle (Sun and McDonough, 1989) and have steep REE profiles with high La/Yb_{PM} (8.4–14.3), high Sm/Yb_{PM} (3.5–4.8) that are similar to typical OIB. The melts also have characteristic deep troughs in Nd, Zr and Hf (Fig. 7). Primitive mantle normalised trace element compositions of the calculated melts overlap (Fig. 7) with the compositions of 29 picrite dykes found throughout the SIP (Reginiussen et al., 1995; Robins, 1975; Robins and Takla, 1979; Yeo, 1984). The key differences are that the picrite dykes have weaker negative anomalies in Zr and Hf and lower LREE/HREE ratios of La/Yb_{PM} of 4.44–11.70 and Sm/Yb_{PM} of 1.96–4.44 compared to the calculated melt compositions. The melts in equilibrium with clinopyroxene also plot within the field of olivine hosted melt inclusions and high-MgO picrite and ferropicrite host magmas from Emeishan (Kamenetsky et al., 2012), Paraná-Etendeka (Gibson, 2002; Jennings et al., 2017; Thompson and Gibson, 2000) and Karoo (Heinonen et al., 2015; Jennings et al., 2017; Riley et al., 2005) CFB provinces (Fig. 8).

7.2. REAFC processes in a deep crustal intrusion

There is abundant field, petrological and geochemical evidence to show that there was a combination of Recharge Assimilation, Fractional Crystallisation, and magma mixing (REAFC) during the formation of the ULS and CS cumulates (Bennett et al., 1986; Emblin, 1985;Grant et al., 2016; Larsen et al., 2018). In this section, we attempt to provide quantitative to semi-quantitative constraints on these processes. Thus far, the trace element composition of the melts in equilibrium with clinopyroxene have been calculated but the major element compositions are still unknown. We opt to use the general numerical REAFC model by Lee et al. (2014) to simultaneously model fractional crystallisation (FC), eruption (E) crustal assimilation (A) and recharge / magma mixing (R) processes. The general numerical model from Lee et al. (2014) can be used for magma chambers of changing mass (growing or dying magma chamber), which is applicable to Reinfjord because the transition from the ULS to CS implies a growing magma chamber and the late dykes suggest a dying magma chamber (Larsen et al., 2018; Orvik, 2019). It is possible that individual cyclic units or series (ULS or CS) in Reinfjord reach a steady state, but in this work, we aim to focus on trends across multiple units and series to understand the macro-scale evolution of the magma chamber.

The results of the models are shown in terms of Sm/Zr vs La to model incompatible element enrichments and the variation in the negative Zr anomalies (Fig. 8). Clinopyroxenes measured in our samples show a range in Sm/Zr from 0.07 to 0.18 and La from 0.6 to 3.3 ppm. The calculated melts in equilibrium with clinopyroxene show a range of 0.032 to 0.064 and La from 11 to 29 ppm. Some of the local picrites from the SIP overlap with our calculated melt compositions but a large group of picrites plot towards lower and less variable Sm/Zr ratios of 0.024–0.034 with La of 10–22 ppm (Fig. 8). These data are compared to models of FC, AFC and magma mixing (RFC). For further details of the compositions, partition coefficients and example calculations are available in the supplementary materials and appendix 2. Two end-member starting melt compositions are chosen. The first melt (named $MELT_{CPX\text{-}0}$) is the most juvenile melt calculated from the clinopyroxene compositions and is the strongest candidate for the most primitive melt to crystallise clinopyroxene, it is La poor and has high Sm/Zr ratios. The second melt is a picrite dyke composition ($MELT_{PIC\text{-}0}$) with one of the lowest concentrations of La (11 ppm), low Sm/Zr (0.027) and highest

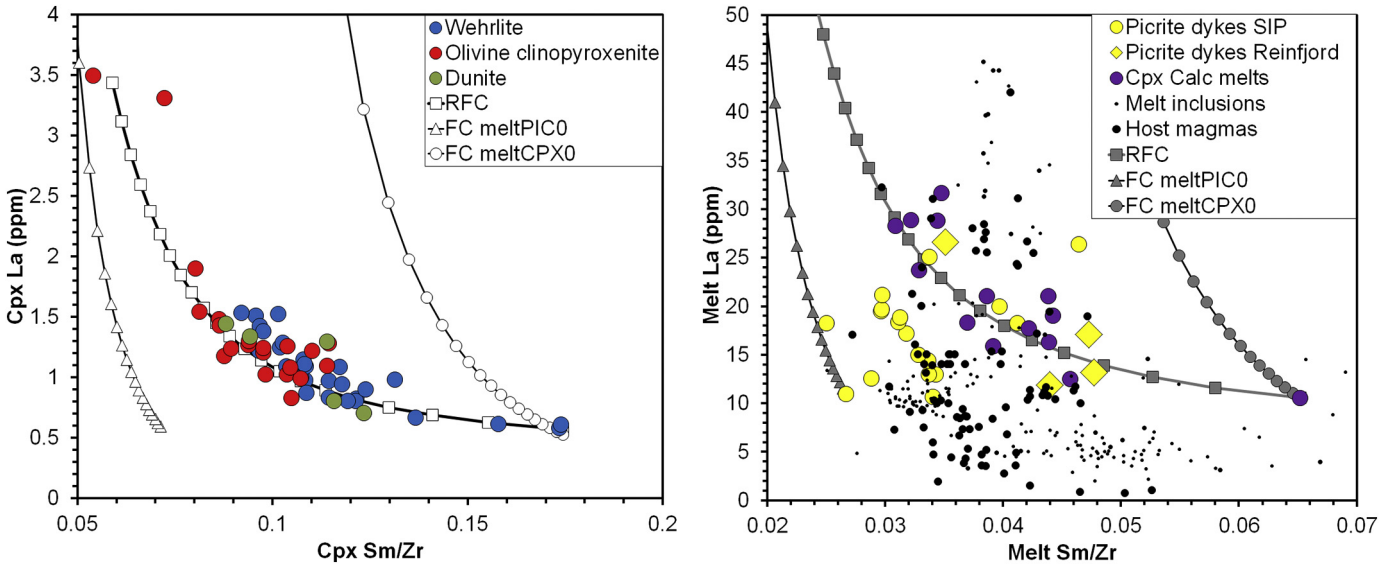

Fig. 8. Results of FC modelling and RFC modelling of parent melt compositions. See text and appendix 2 for further details. Left panel - is clinopyroxene compositions from dunite, wehrlite and olivine clinopyroxenite from Reinfjord. Right panel shows local picrite dykes from the SIP (Reginiussen et al., 1995; Robins, 1975; Robins and Takla, 1979; Yeo, 1984), calculated melt compositions in equilibrium with clinopyroxene from Reinfjord, high-MgO magmas from Emeishan (Kamenetsky et al., 2012), Paraná-Etendeka (Gibson, 2002; Jennings et al., 2017; Thompson and Gibson, 2000) and Karoo (Heinonen et al., 2015; Jennings et al., 2017; Riley et al., 2005). Yellow diamonds are picrites from the drill cores from Reinfjord (see supplementary material for full compositions). FC MELTCPX-0 and FC MELTPIC0 are lines of fractional crystallisation of $MELT_{CPX\text{-}0}$ and $MELT_{PIC0}$ respectively, where each point represents 5% fractional crystallisation where the mass of crystals removed (∂M_x) = −0.05. RFC is a recharge and crystallisation model where the mass of recharging magma (∂M_{re}) = 0.07 and ∂M_x = −0.1, meaning that each point represents 3% fractional crystallisation. (For interpretation of the references to colour in this figure legend, the reader is referred to the web version of this article.)

MgO (16.21 wt%), Ni (388 ppm) and Cr (1594 ppm) from Reginiussen et al. (1995). The picrite dykes from the SIP have previously been thought to be the parent magmas that formed the ultramafic intrusions (Bennett et al., 1986; Emblin, 1985;Grant et al., 2016; Larsen et al., 2018) and they are not contaminated by continental crust (Reginiussen et al., 1995).

7.2.1. Fractional crystallisation (FC)

During fractionation of olivine and/or olivine + clinopyroxene, Sm and Zr are not strongly fractionated from each other but La, which is very incompatible in both phases, increases rapidly with each degree of fractional crystallisation. Fractional crystallisation therefore cannot produce the observed range in Sm/Zr observed in our calculated melt compositions or measured clinopyroxene compositions (Fig. 8) but could explain the chemical variation in some of the picrite dykes that show limited variation in Sm/Zr and enrichments in La.

7.2.2. Assimilation and fractional crystallisation (AFC)

Assimilation of the layered gabbroic wall-rocks is common in the marginal zones of Reinfjord and throughout the other ultramafic intrusions in the SIP (Bennett et al., 1986; Emblin, 1985; Grant et al., 2016; Griffin et al., 2013; Larsen et al., 2018; Sturt et al., 1980,). The ULS and CS (particularly our samples) do not display field and petrographic indicators of contamination such as recrystallised gabbro xenoliths, hybrid pyroxenite rocks and plagioclase bearing peridotites, nor do they show whole rock geochemical signatures of contamination such as increasing Al_2O_3 with decreasing Cr_2O_3 (Grant et al., 2016; Larsen et al., 2018). Nevertheless, subtle geochemical signatures of assimilation have not been explored. The wall-rock mafic rocks vary significantly due to modal layering and variable contamination from metasedimentary country-rocks. To explore the effects of contamination by partial melts of gabbro we used two bulk rock gabbro-norite compositions from Grannes (2016), mineral proportions calculated using a CIPW norm and partition coefficients for plagioclase, orthopyroxene and clinopyroxene collated from Bédard (1994), Bindeman et al. (1998), and Adam and Green (2006). Details are provided in the supplementary materials and some uncertainties are discussed in Appendix 2. The incoming ultramafic melts are likely to have had temperatures of up to or even greater than 1450 °C (Larsen et al., 2018), meaning that they could have been several hundred degrees above the solidus of the wall-rock gabbro-norite. Short time spans between mafic and ultramafic magmatism may also mean that the gabbro-norites were well above the ambient crustal temperatures and close to their solidus (Larsen et al., 2018). The degrees of partial melting were therefore potentially high, and this is corroborated by the field relationships of the marginal zones (Larsen et al., 2018). Therefore, the estimated partial melt compositions of grabbro-norite were calculated using melt fractions of 0.1, 0.2 and 0.3 (see supplementary materials 4).

None of the AFC models provided a good fit for the measured clinopyroxene compositions. Changes in the amount of contaminant added relative to amount of crystallisation removed, do move the model AFC curves towards the clinopyroxene compositions, but begin to face the issue that a very large amount of gabbro-norite must have been assimilated, for which there is little field, geochemical, (Bennett et al., 1986; Emblin, 1985; Grant et al., 2016; Larsen et al., 2018) or sulphur-isotope (Larsen et al., 2019) evidence for. The partial melt compositions have generally too high Sm/Zr and high La to result in the clinopyroxene compositions observed that stretch to very low Sm/Zr at moderate La compositions. As Sm is not strongly fractionated from Zr during partial melting of plagioclase, orthopyroxene and clinopyroxene the Sm/Zr ratio in partial melts is close to that of the original gabbro-norite. It is possible that small amounts of contamination by partial melts of the gabbro-norite contributed to the variations in clinopyroxene but are unlikely to drive the trend of rapidly decreasing Sm/Zr ratios over moderate increases in La. The early development of thick marginal zones, appears therefore to shield the incoming ultramafic melts from further contamination by acting as a mechanical and chemical barrier, as expected by REAFC modelling in other LIP regions (Yu et al., 2015).

7.2.3. Recharge and fractional crystallisation (magma mixing scenario)

The evolution of the Reinfjord magma chamber involved a main phase of magma chamber growth through injection of high-MgO magmas that resulted in increasing temperatures, MgO contents and a "reverse crystallisation sequence" of pyroxenite marginal zones- > olivine clinopyroxenite and wehrlite ULS- > dunites in the CS (Grant et al., 2016; Larsen et al., 2018). Multiple, sharp reversals in olivine compositions and bulk rock compositions from drill cores, widespread field evidence of replacive dunites and intrusive *syn*-magmatic pyroxenitic bodies all indicate repetitive magma recharge events (Grant et al., 2016; Larsen et al., 2018). Larsen et al. (2018) also demonstrated that the Reinfjord magma chamber accommodated a diverse suite of magma compositions including high-MgO picrite-komatiites, carbonatites and alkaline melts within a very short space of time (<10 Ma), raising the possibility of mixing of very different melt compositions. However, mixing with carbonatites (Røisi, 2018) and alkali rocks in the SIP, which have high Sm/Zr ratios (up to 0.3) and high La (~587 ppm) and tend to appear late in the evolution of Reinfjord, cross-cutting most other features, clearly could not produce the observed decreasing Sm/Zr with increasing La trend (Fig. 8) in our clinopyroxenes.

In recharging (RFC) magma chambers, for each overturn (each recharge event over a fractionation interval), incompatible elements become more enriched than less incompatible and compatible elements compared to fractional crystallisation alone (Lee et al., 2014). Recharge would therefore be expected to lower the Sm/Zr ratio because Sm is approximately 3 times more compatible than Zr in clinopyroxene. Recharge of the same melt composition, i.e. the initial melt and recharging melt compositions are both $MELT_{CPX\text{-}0}$, results in a stronger decrease in Sm/Zr for a given La compared to fractional crystallisation, but not by enough to replicate the clinopyroxene compositions measured in our samples.

To model recharge of different magma compositions, we take $MELT_{CPX\text{-}0}$ (with low La and high Sm/Zr) as the initial magma composition and $MELT_{PIC0}$, a primitive local picrite with low La and low Sm/Zr from Reginiussen et al. (1995), as the recharging melt composition. Recharge and mixing of $MELT_{CPX\text{-}0}$ and $MELT_{PIC0}$ can reproduce the observed clinopyroxene compositions over a range of ∂M_{re} (change in mass due to recharge) to dM_x (change in mass due to crystallisation) ratio (e.g. $\partial M_{re}/\partial M_x = 0.3$–$0.9$), where ratios of 0.5–0.7 are regarded as the best fit on the grounds that they are closest to a polynomial fit ($R^2 = 0.83$) of the clinopyroxene compositions (supplementary materials 4).

The results indicate that our clinopyroxenes formed over a fractionation interval of approximately 35%, consistent with experimental studies on picrite melts at ~1 GPa (Müntener and Ulmer, 2006; Tuff et al., 2005). The mixed melt RFC model produces melt compositions that have the similar Sm/Zr vs La of those calculated from clinopyroxene from Reinfjord and some of the picrite dykes from the SIP (Fig. 8), particularly four dyke compositions found within the drill cores from Reinfjord (supplementary materials, Fig. 8). Both of the melts involved in the recharge model (RFC) are primitive (i.e. low in REE) and would maintain high temperatures, high MgO contents and keep the melts either on the olivine liquidus or olivine + clinopyroxene cotectic for longer than fractional crystallisation alone, allowing for the formation of thick ultramafic units (e.g. CS >700). Additionally, this model can account for reverse zoned clinopyroxenes in some of our samples (e.g. in LA11005 and LA11009), if $M_{re} >> M_x$, i.e. magma chamber expansion through higher rates of recharge than crystallisation, and the recharging magma changes from $MELT_{PIC0}$ to $MELT_{CPX\text{-}0}$. We therefore propose that the ULS and CS cumulates in Reinfjord predominantly formed through mixing and fractional crystallisation of ultramafic magmas with varying compositions that were similar to $MELT_{CPX\text{-}0}$ and $MELT_{PIC0}$.

7.3. Characterising the mantle beneath the SIP

7.3.1. A volatile-bearing asthenosphere

To date, the composition of the mantle beneath the SIP is poorly constrained because of a lack of geochemical and isotopic data for many of the intrusions. However, it is possible to make some inferences from the available data. Mafic, ultramafic, alkaline and carbonatite intrusions have depleted mantle isotopic ($^{87}Sr/^{86}Sr$;0.7038, ε_{Nd};+4, and ε_{Hf};+8) compositions and show varying degrees of contamination by Archean continental crust (Griffin et al., 2013; Mørk and Stabel, 1990; Roberts, 2010; Tegner et al., 1999). The high ε_{Nd} and ε_{Hf}, and low $^{87}Sr/^{86}Sr$ overlap with MORB and OIB compositions and are consistent with magma generation within the upwelling asthenospheric mantle with limited contribution from a metasomatised sub-continental lithospheric mantle (SCLM). Carbonatite and alkaline intrusions with distinctly mantle isotopic compositions in $\partial^{13}C$ (−6 to −8‰), $\partial^{18}O$ (+6 to +8‰), ε_{Nd} of +4 and ε_{Hf} of +8 (Roberts et al., 2010; Wulff-Pedersen, 1992), occur with or shortly before (Sørøya alkaline complex)

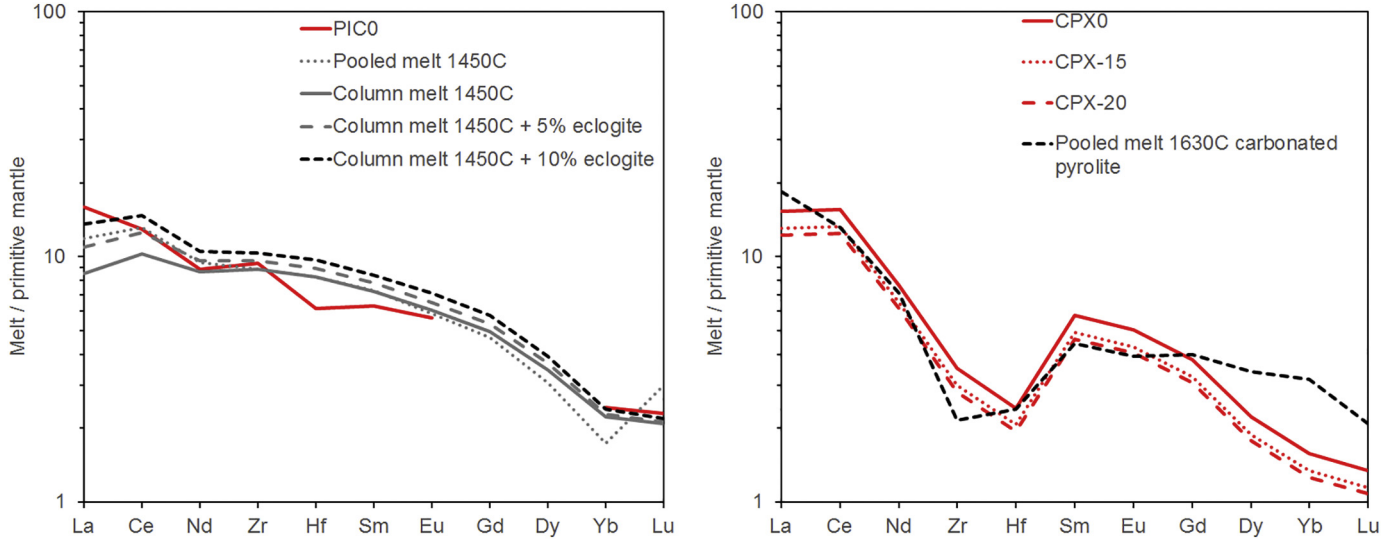

Fig. 9. Primitive mantle normalised melt compositions produced by modelling using REEBOX PRO (Brown and Lesher, 2016). For further details see text and appendix 3. (For interpretation of the references to colour in this figure legend, the reader is referred to the web version of this article.)

Table 2
All values are normalised to primitive mantle (Sun and McDonough, 1989). Comparison between local SIP picrite (from Reginiussen et al., 1995) and melts calculated to be in equilibrium with clinopyroxene from Reinfjord with melt compositions from mantle melting models. PIC 0 = local SIP picrite, CPX-0 = most primitive melt in equilibrium with clinopyroxene from Reinfjord, CPX-15 = CPX-0 back calculated by addition of 15 wt% olivine, and CPX-20 = CPX-0 back calculated by addition of 20 wt% olivine using partition coefficients of Bédard, 1994 (See supplementary materials). WH DMM = DMM trace element composition from Workman and Hart (2005) and G13 NMORB = NMORB trace element composition from Gale et al. (2013). Carbonated peridotite composition was calculated binary mixing of depleted mantle (Hofmann, 1988) and the average of 4 bulk rock carbonatite (all of which have mantle isotopic signatures and are thought to originate from the mantle – Larsen et al., 2018) compositions from SIP (Røisi, 2018). For more information on the "Default" partition coefficients used in REEBOX PRO the reader is referred to Brown and Lesher (2016).

	PIC0	"Normal" Asthenosphere				CPX0	CPX-15	CPX-20	"Carbonated" Peridotite
Pooled / column melts		pool	column	column	column				column
Lithology/ies		pyrolite	pyrolite	pyrolite + G2 pyroxenite	pyrolite + G2 pyroxenite				DM + carbonatite
Partition coefficients		default	default	default	default				Dasgupta et al. (2009)
G2 pyroxenite (%)		0	0	5	10				0
Peridotite/pyroxenite TE		WH DMM	WH DMM	WH DMM/G13 NMORB	WH DMM/G13 NMORB				Carbonated peridotite
Water (ppm)		0	0	0	0				250
T_P °C		1450	1450	1450	1450				1630
La	16.01	11.88	8.54	10.97	13.65	15.35	13.05	12.28	18.44
Ce	12.96	13.18	10.24	12.52	14.78	15.57	13.23	12.46	13.18
Nd	8.86	9.46	8.68	9.64	10.5	7.67	6.52	6.13	7.13
Zr	9.38	8.91	8.89	9.6	10.33	3.52	2.99	2.81	2.15
Hf	6.15	8.28	8.26	8.99	9.72	2.41	2.06	1.94	2.38
Sm	6.31	7.28	7.21	7.82	8.43	5.78	4.91	4.62	4.41
Eu	5.65	5.88	6.03	6.52	7.08	5.05	4.29	4.04	3.93
Gd	–	4.7	4.96	5.34	5.77	3.82	3.24	3.05	3.99
Dy	–	3.07	3.46	3.67	3.94	2.21	1.88	1.77	3.39
Yb	2.43	1.74	2.23	2.28	2.39	1.57	1.34	1.26	3.17
Lu	2.3	3	2.08	2.11	2.18	1.34	1.14	1.08	2.09

or after (Lillebukta alkaline complex) several of the major ultramafic intrusions in the SIP (Larsen et al., 2018; Larsen et al., 2019), including Reinfjord, indicate prolonged production of volatile enriched magma compositions from the mantle. The ultramafic intrusions show a crystallisation sequence where clinopyroxene and amphibole appear before plagioclase that is characteristic of the liquid line of descent for a wet magma in the lower crust (e.g. Müntener and Ulmer, 2006). Sulphides from the Reinfjord intrusion, comprising 1–2% of the cumulates, have mantle values $\delta^{34}S$ of −2 to +2‰ and therefore indicate that the parent melts were also relatively sulphur-rich and that the source of S was the mantle and not from contamination by crustal sediments that in the country-rock metasediments gave a value of $+9^{o}/_{oo}$(Larsen et al., 2018, 2019). Together, the isotopic data suggests a volatile enriched asthenospheric mantle source for the SIP.

7.3.2. Origin of the ultramafic high-MgO magmas in Reinfjord

To provide better constraints on the melting conditions and mantle souces of the ultramafic melts in the Reinfjord intrusion ($MELT_{CPX-0}$ and $MELT_{PIC0}$) we use the REEBOX PRO (Brown and Lesher, 2016) forward model of adiabatically upwelling asthenospheric mantle. Details of the REEBOX PRO modelling are outlined in Appendix 3. $Melt_{PIC-0}$ as well as other picrite dykes in the SIP appear to be very similar to melts formed by melting of a typical asthenospheric peridotite source containing up to 10% pyroxenite (Fig. 9a, Table 2). In these models, the mantle potential temperatures are around 1450 °C with pressures of initial melting being ~4.5 GPa for the pyroxenite bearing sources (~3.6 GPa for the pyroxenite-free source). $MELT_{CPX-0}$ and back calculated compositons by olivine addition, $MELT_{CPX-10}$ and $MELT_{CPX-15}$ (see supplementary materials) are compositionally closely modelled by melting of a carbonated peridotite without pyroxenite (Fig. 9b, Table 2). In this case, mantle potential temperatures are up to 1630 °C and depths of intitial melting are ~7 GPa. The presence of carbonated peridotite in the mantle beneath the SIP would be consistent with the presence of carbonatites with mantle isotopic signatures (Roberts et al., 2010) and the widespread occurence of carbonatites of similar ages in the CIMP (Ernst and Bell, 2010; Tappe et al., 2011).

7.3.3. A thermally and compositionally heterogeneous mantle plume

The SIP is spatially and temporally correlated with prolonged (616–560 Ma), voluminous, and widespread magmatism across Laurentia and Baltica known as the CIMP. The CIMP includes numerous intrusions, dyke swarms (e.g. Andréasson et al., 1998; Hollocher et al., 2007; Tegner et al., 2019 for dyke swarms in Scandinavia) carbonatites and kimberlites (Ernst and Bell, 2010; Tappe et al., 2011), which originated from diverse asthenospheric mantle sources, thermal anomalies (i.e. multiple mantle plumes) and thining of the continental lithoshpere. Our REEBOX modelling indicates that the ultramafic magmas in the SIP were derived from fractional melting of an asthenospheric mantle source that was dominated by ambient DMM with varying amounts of recycled oceanic crust and carbonatite metasomatised peridotite. The high mantle potential temperatures (up to 1630 °C) indicate the presence of a significant thermal anomaly, supporting earlier claims of the impingement of a deep mantle plume on the lithosphere beneath the SIP (Bennett et al., 1986; Griffin et al., 2013; Larsen et al., 2018; Robins and Gardner, 1975). The earlier (615–590 Ma) Scandinavian dyke swarms, which are correlated with the SIP (Andréasson et al., 1998; Tegner et al., 2019) record lateral compositional variations in the mantle plume with more enriched mantle sources in the south (e.g. Egersund dyke swarm - Bingen and Demaiffe, 1999, Tegner et al., 2019) and more depleted mantle sources in the North (e.g. the Corrovarre dyke swarm Tegner et al., 2019). Our results correlate well with the southern segment of the Scandinavian dykes swarms, however, the SIP records a far greater diversity of magmas within a shorter space of time (<10–20 Ma) and areal extent compared to the Scandinavian dyke swarms. It is possible that the Seiland plume was more heterogeneous compared to that which formed the Scandinavian dyke swarms and actually correlates more strongly with West Greenland kimberlites in terms of age (568–553 Ma), depth of melting (>6 GPa) of carbonate-bearing asthenospheric periodite, negative Zr—Hf anomalies and juvinile ε_{Hf} values of +4 and ε_{Nd} of +3 (Tappe et al., 2011).

8. Conclusions

The Reinfjord ultramafic intrusion, SIP, represents a deep crustal volcanic conduit system that was part of and arguably fed a LIP. The

intrusion provides rare insights into the ascent and modification of primary mantle-derived ultramafic magmas at the base of the crust.

Clinopyroxenes from dunite, wehrlite and olivine clinopyroxenites were analysed for their trace element compositions using LA-ICP-MS and major elements using EPMA. The data is then used to calculate clinopyroxene composition specific partition coefficients using the parameterizations of Bédard (2014). The partition coefficients were then used to determine the composition of the melts that were in equilibrium with the clinopyroxenes, which represent a close approximation to the parent melts that formed the intrusion. The melts have steep REE profiles with high LREE/HREE (e.g. La/Yb_{PM} of 8.4–14., Sm/Yb_{PM} of 3.5–4.8) and negative anomlies in Zr, Hf and Nb. Using trace element ratios and the formulations for a magma chamber that is changing in mass and undergoing combined REAFC process (Lee et al., 2014), we find that the compositions of the clinopyroxenes and their equilibirum melts can be formed by a combination of recharge and mixing of two end-member melt compositions. The first ($MELT_{CPX\text{-}0}$) end-member has steeper LREE/HREE and deeper anomalies in Zr and Hf, and the second end-member ($MELT_{PIC0}$) is similar to primitive picrite dykes from the SIP, which have less steep LREE/HREE and less pronounced anomalies in Zr and Hf. Our results imply that the central zones of the magma conduit system are domianted by recharge, magma mixing and fractional crystallisation with a minimal input from crustal contamination.

Finally, we use forward modelling of adiabatically upwelling mantle with heterogenous lithologies in the REEBOX PRO melting model to explore the mantle conditions that produced the range in the compositions of ultramafic magmas that entered the Reinfjord intrusion. The results indicate that $MELT_{CPX\text{-}0}$ formed by melting of carbonate metasomatised peridotite with mantle potential temperatures of 1630 °C and that $MELT_{PIC0}$ formed by melting of a peridotite source with up to 10% pyroxenite component and mantle potential temperatures of up to 1450 °C. These results indicate a compositionally and thermally inhomogeneous mantle plume beneath the SIP, which produced two distinct end-member magma series.

Declaration of Competing Interest

None

Acknowledgements

This research was funded from the People Programme (Marie Curie Actions) of the European Union's Seventh Framework Programme FP7/2007-2013/ under REA – Grant Agreement n°608001. The Nordic Council of Ministers secured continuation of the project in 2013-16 through the NorMin funding scheme (No 14814103) by supporting a research drilling project (RF-3 and 4). Additional support and project costs came from the Norwegian Geological Survey (NGU) in order to obtain LA-ICP-MS data. The authors would like to thank Oddmund Hansen and the people of Reinfjord for their logistical support and hospitality, without which the field work would not have been possible. Constructive comments from Eleanor Jennings and an unnamed reviewer as well as the editorial handling greatly improved the original manuscript and we are greatful for thier efforts. A personal thank you is given to Håkon and Fredrik.

Appendix 1 – Derivation of partition coefficients for calculating the composition of melts in equilibrium with clinopyroxene

The composition of melts in equilibrium with the clinopyroxenes from Reinfjord can be estimated using appropriate partition coefficients. Partition coefficients depend strongly on the composition of the clinopyroxene, the melt, temperature and pressure. The parameterizations in Bédard et al. (2014) allow us to calculate appropriate clinopyroxene-melt partition coefficients. The estimates for the pressures (6.8–9 kbar) and temperatures (>1300 °C see above) of crystallisation at Reinfjord (Grant et al., 2016) are not precise enough be used for these calculations. The R^2 values for the linear regressions for pressure or temperature are also typically low. To achieve better results, we calculated the partition coefficients for each element using the amount of tetrahedral Al in the clinopyroxene (Supplementary materials). The concentrations of Al^{IV}, determined from the EPMA data are also much more accurate than pressure or temperature estimates. As we do not know the SiO_2, we used the lowest likely SiO_2 (37 wt%) from the dunite melts (Griffin et al., 2013) and the most Si_2O-rich picrite dyke (<49 wt%) from Reginiussen et al. (1995). Using these values, the $D_{Ti}^{Cpx/melt}$ is calculated using equation number 80op (for SiO_2 = 35–39.99 wt%) and equation number 80 l (for SiO_2 = 45–49.99 wt%) from Bédard et al. (2014). Partition coefficients for REE and HFSE were then calculated using the slope and intercept values for $D_{Ti}^{Cpx/melt}$ vs $D_i^{Cpx/melt}$ from Bédard (2014). The calculated partition coefficients are then compared to experimental values given in Bédard (1994). Example calculations are shown in Table A1.

	REE measured	Data from Bédard (2014)		kD (calculated)			Calculated melt compositions		
		Slope	Intercept	Melt SiO2 = 47–49.99	Melt SiO2 = 35–39.99	Bédard, 1994	Melt SiO2 = 47–49.99	Melt SiO2 = 35–39.99	Bédard, 1994
Ti				0.364	0.383				
La	0.583	−1.723	1.158	0.055	0.059	0.054	10.55	9.93	10.87
Ce	2.552	−1.213	1.155	0.092	0.098	0.086	27.63	26.02	29.75
Nd	2.123	−0.356	1.217	0.205	0.218	0.187	10.38	9.74	11.33
Zr	4.580	−0.999	1.139	0.116	0.123	0.123	39.37	37.11	37.11
Hf	0.171	1.027	−1.475	0.229	0.241	0.256	0.75	0.71	0.67
Sm	0.794	−0.162	0.999	0.309	0.326	0.291	2.57	2.44	2.73
Eu	0.268	0.008	1.146	0.316	0.335	0.329	0.85	0.80	0.82
Gd	0.904	−0.060	0.853	0.397	0.415	0.367	2.27	2.18	2.46
Dy	0.806	0.223	0.917	0.494	0.518	0.442	1.63	1.56	1.82
Yb	0.379	0.297	1.000	0.489	0.516	0.430	0.78	0.74	0.88
Lu	0.047	−0.017	0.726	0.472	0.490	0.433	0.10	0.10	0.11

*Units are in ppm, except for kD values that are dimensionless.

Appendix 2 - Recharge, eruption, assimilation, fractional crystallisation (REAFC) models

REAFC calculations use the formulation of a magma chamber that is changing in mass where it is possible to simultaneously simulate recharge, evacuation, assimilation, and fractional crystallisation. For further details on this approach the reader is referred to Lee et al. (2014) and example calculations can be found in the supplementary materials. The composition of the magma in the magma chamber, for a given element, is calculated as follows;

$$C_{ch} = (C_{ch} \times \partial M_{ch} + C_{re} \times \partial M_{re} + C_x \times \partial M_x + C_{ch} \times \partial M_e + C_{cc} \times \partial M_{cc})/M_{ch}$$

Where C_{ch} is the composition of magma in the magma chamber, C_{re} is the composition of recharged magma, C_x is the composition of crystallised materials which are calculated using C_{ch} x D (partition coefficient), C_e is the composition of erupted magma, C_{cc} is the composition of contaminant melts (e.g. continental crust or mafic wall-rocks). M_{re} is the mass of recharging melt entering the magma chamber, M_x is the mass of crystallised material, M_e is the mass of magma erupting from the magma chamber, M_{cc} is the mass of contaminating melts entering the magma chamber, and M_{ch} is the change in mass of the magma chamber (the product of M_{re}, M_x, M_e, and M_{cc}). For all models, the clinopyroxene partition coefficients used were the averages of those calculated in appendix 1 using the parameterization from Bédard (2014) and the measured clinopyroxene compositions in our samples. The partition coefficients were as follows; $D_{Zr}^{Cpx/melt} = 0.11$, $D_{La}^{Cpx/melt} = 0.05$ $D_{Sm}^{Cpx/melt} = 0.31$ $D_{Yb}^{Cpx/melt} = 0.48$.

For fractional crystallisation models, the ∂M_{re}, ∂M_{cc} and ∂M_e were set to 0 and two different parent melt compositions were used; the most REE-poor melt in equilibrium with clinopyroxene from Reinfjord ($MELT_{CPX\text{-}0}$) and a primitive picrite dyke composition from the SIP ($MELT_{PIC0}$). During the formation of the CS and ULS cumulates, the Reinfjord magma chamber was expanding due to high influx of magma relative to eruption of magma (Grant et al., 2016; Larsen et al., 2018), i.e. $\partial M_{re} > \partial M_e$. For simplicity, the values of ∂M_e and ∂M_{cc} in the RFC modelling were therefore set to 0. For AFC modelling, the C_{cc} is calculated using fractional melting of two gabbro-norite compositions from Grannes (2016) at melt fractions of 0.1, 0.2, and 0.3. Uncertainties in the mineral modes of the gabbro-norite samples and the modal contribution of each phase to the melt in non-modal melting have relatively small effects on the calculated melt compositions. For example, melt modes of 0.45 clinopyroxene, 0.45 orthopyroxene and 0.1 plagioclase (which would form residual anorthosites like those observed in the field) with KG14011 and a melt fraction of 0.3 gives almost identical La concentrations and less than 5% difference in the Sm/Zr ratio when compared with modal melting of CIPW norm determined modes of 0.15 clinopyroxene, 0.18 orthopyroxene and 0.53 orthopyroxene. This is because Sm and Zr are not strongly fractionated from each other by melting plagioclase-orthopyroxene-clinopyroxene dominated cumulates and La being highly incompatible in all phases. As detailed studies of the mineral chemistry of the gabbro-norite samples are lacking, mineral – melt composition specific partition coefficients could not be estimated.

Appendix 3 - REEBOX PRO modelling

To model the melting conditions that could give rise to the calculated parental magma compositions, we utilised the REEBOX PRO melting model (Brown and Lesher, 2016). This forward model simulates adiabatic decompression melting of lithologically homogeneous and heterogeneous sources containing anhydrous/hydrous peridotite ± pyroxenite. Model inputs include the mantle potential temperature, initial trace element composition (s) of the source lithology/ies, and the thickness of any pre-existing continental lithosphere. The model outputs the compositions of all instantaneous melts generated by each lithology during each decompression step, as well as the melt compositions resulting from accumulating all instantaneous melts along the melting column (column-accumulated melts) and pooling all column-accumulated melts to form the bulk crust.

We first ran models for "typical" asthenospheric conditions assuming melting of an anhydrous pyrolite peridotite mantle that contained 0, 5, or 10% recycled oceanic crust (G2 pyroxenite). G2 pyroxenite is an experimental composition devised in (Pertermann et al., 2004; Pertermann and Hirschmann, 2003) and has been referred to as both eclogite and pyroxenite. We refer to all clinopyroxene + garnet-rich lithologies as pyroxenite. In each of these models, we utilised the default temperature-dependent mineral-melt partition coefficients for peridotite (and default pyroxenite mineral-melt partition coefficients), and assumed the peridotite had an initial trace element composition of depleted MORB mantle (DMM; Workman and Hart, 2005), whereas the pyroxenite had an initial trace element composition of normal MORB (Gale et al., 2013). Although the thickness of the lithosphere during the emplacement of the SIP remains poorly constrained, we assumed a lithospheric thickness of 100 km in all models based upon the similarity of olivine Mn contents (most primitive = 0.15 wt% Mn) from Grant et al. (2016) to the "thick-lithosphere" olivines identified by Sobolev et al. (2007).

The carbonatite intrusions in the SIP have depleted mantle isotopic signatures and are temporally and spatially linked to carbonatites from the CIMP (Ernst and Bell, 2010). The latter have been shown to have formed from partial melting of a volatile enriched mantle source. (e.g. W. Greenland; Tappe et al., 2011) We therefore also ran models simulating melting of carbonatite metasomatised peridotite. The onset of carbonated peridotite melting is significantly deeper than that of anhydrous peridotite melting (e.g. Brey et al., 2007; Falloon and Green, 1989), so we simulated this deeper onset of melting using the hydrous peridotite melting capabilities in REEBOX PRO (which does not yet have the capability of modelling carbonated peridotite melting). Strictly speaking, the depth for the onset of melting, and the melting functions of hydrated and carbonated peridotite are not identical (e.g. Dasgupta, 2018). However, the key similarity between the two is the generation of low degree melts at greater depths than anhydrous peridotite melting. Because we are modelling the compositions of all instantaneous melts accumulated over the entire length of the melting column, and pooled melt compositions (derived from everywhere in the melting zone), any potential differences in the low degree melt compositions arising from differences in the depth of initial melting and/or melting behavior of carbonated and hydrous peridotite are minimal. As carbonated peridotite melting also affects mineral-melt elemental partitioning, we utilised the carbonated peridotite mineral-melt partition coefficients of Dasgupta et al. (2009) in these sets of calculations. The intial trace element composition of the model carbonated peridotite source is a mixture of 0.5% of the average composition of carbonatites from Røisi (2018) and 99.5% primitive mantle (Hofmann, 1988).

	Depleted mantle + carbonatite	Carbonatite (Røisi, 2018)	Hofmann DM
La	3.55	587.00	0.61
Ce	6.78	1038.00	1.60
Nd	2.90	344.00	1.19
Zr	10.41	148.12	9.71
Hf	0.29	3.91	0.27
Sm	0.60	42.60	0.39
Eu	0.20	10.50	0.15
Gd	0.68	34.10	0.51
Tb	0.11	3.10	0.09
Dy	0.67	7.50	0.64
Ho	0.15	1.90	0.14
Er	0.44	5.40	0.42
Yb	0.43	3.30	0.41
Lu	0.07	0.70	0.06

Appendix A. Supplementary data

Supplementary data to this article can be found online at https://doi.org/10.1016/j.lithos.2020.105535.

References

Adam, J., Green, T., 2006. Trace element partitioning between mica-and amphibole-bearing garnet lherzolite and hydrous basanitic melt: 1. Experimental results and the investigation of controls on partitioning behaviour. Contrib. Mineral. Petrol. 152, 1–17.

Andréasson, P., Svenningsen, O.M., Albrecht, L., 1998. Dawn of phanerozoic orogeny in the North Atlantic tract; evidence from the Seve-Kalak superterrane, Scandinavian Caledonites. GFF 120, 159–172.

Bédard, J.H., 1994. A procedure for calculating the equilibrium distribution of trace elements among the minerals of cumulate rocks, and the concentration of trace elements in the coexisting liquids. Chem. Geol. 118, 143–153.

Bédard, J.H., 2001. Parental magmas of the Nain Plutonic Suite anorthosites and mafic cumulates: a trace element modelling approach. Contrib. Mineral. Petrol. 141, 747–771.

Bédard, J.H., 2005. Partitioning coefficients between olivine and silicate melts. Lithos 83, 394–419.

Bédard, J.H., 2014. Parameterizations of calcic clinopyroxene–Melt trace element partition coefficients. Geochem. Geophys. Geosyst. 15, 303–336.

Bennett, M.C., Emblin, S.R., Robins, B., Yeo, W.J.A., 1986. High-temperature ultramafic complexes in the North Norwegian Caledonides: I – Regional setting and field relationships. Norges Geol. Unders. Bull. 405, 1–41.

Berly, T.J., Hermann, J., Arculus, R.J., Lapierre, H., 2006. Supra-subduction zone pyroxenites from San Jorge and Santa Isabel (Solomon Islands). J. Petrol. 47, 1531–1555.

Bindeman, I.N., Davis, A.M., Drake, M.J., 1998. Ion microprobe study of plagioclase-basalt partition experiments at natural concentration levels of trace elements. Geochim. Cosmochim. Acta 62, 1175–1193.

Bingen, B., Demaiffe, D., 1999. Geochemical signature of the Egersund basaltic dyke swarm, SW Norway, in the context of late-Neoproterozoic opening of the Iapetus Ocean. Nor. Geol. Tidsskr. 79, 69–86.

Brey, G.P., Bulatov, V.K., Girnis, A.V., Lahaye, Y., 2007. Experimental Melting of Carbonated Peridotite at 6–10 GPa. J. Petrol. 49, 797–821.

Brown, E.L., Lesher, C.E., 2016. REEBOX PRO: A forward model simulating melting of thermally and lithologically variable upwelling mantle. Geochem. Geophys. Geosyst. 17, 3929–3968.

Bryan, S.E., Ernst, R.E., 2008. Revised definition of large igneous provinces (LIPs). Earth Sci. Rev. 86, 175–202.

Corfu, F., Roberts, R.J., Torsvik, T.H., Ashwal, L.D., Ramsay, D.M., 2007. Peri-Gondwanan elements in the Caledonian Nappes of Finnmark, Northern Norway: Implications for the paleogeographic framework of the Scandinavian Caledonides. Am. J. Sci. 307, 434–458.

Dasgupta, R., 2018. Volatile-bearing partial melts beneath oceans and continents–Where, how much, and of what compositions. Am. J. Sci. 318, 141–165.

Dasgupta, R., Hirschmann, M.M., McDonough, W.F., Spiegelman, M., Withers, A.C., 2009. Trace element partitioning between garnet lherzolite and carbonatite at 6.6 and 8.6 GPa with applications to the geochemistry of the mantle and of mantle-derived melts. Chem. Geol. 262, 57–77.

Emblin, S.R., 1985. The Reinfjord ultramafic complex, Seiland Province: emplacement history and magma chamber model. Unpublished Ph.D. thesis. University of Bristol, U.K.

Ernst, R.E., 2014. Large igneous provinces. Cambridge University Press.

Ernst, R.E., Bell, K., 2010. Large igneous provinces (LIPs) and carbonatites. Mineral. Petrol. 98, 55–76.

Falloon, T.J., Green, D.H., 1989. The solidus of carbonated, fertile peridotite. Earth Planet. Sci. Lett. 94, 364–370.

Flem, B., Bédard, L.P., 2002. Determination of trace elements in BCS CRM 313/1 (BAS) and NIST SRM 1830 by inductively coupled plasma-mass spectrometry and instrumental neutron activation analysis. J. Geostandards Geoanal. 26, 287–300.

Gale, A., Dalton, C.A., Langmuir, C.H., Su, Y., Schilling, J.G., 2013. The mean composition of ocean ridge basalts. Geochem. Geophys. Geosyst. 14, 489–518.

Gibson, S.A., 2002. Major element heterogeneity in Archean to Recent mantle plume starting-heads. Earth Planet. Sci. Lett. 195, 59–74.

Grannes, K.R.B., 2016. Cryptic Variations of Olivine and Clinopyroxene in the RF-4 Drill-Core:-A geochemical study of the Reinfjord Ultramafic Complex, Norway. Master's thesis, NTNU (unpublished). https://ntnuopen.ntnu.no/ntnu-xmlui/handle/11250/2420895.

Grant, T.B., Larsen, R.B., Anker-Rasch, L., Grannes, K.R., Iljina, M., McEnroe, S., Nikolaisen, E., Schanche, M., Øen, E., 2016. Anatomy of a deep crustal volcanic conduit system; the Reinfjord Ultramafic Complex, Seiland Igneous Province, northern Norway. Lithos 252, 200–215.

Griffin, W.L., Sturt, B.A., O'Neill, C.J., Kirkland, C.L., O'Reilly, S.Y., 2013. Intrusion and contamination of high-temperature dunitic magma: the Nordre Bumandsfjord pluton, Seiland, Arctic Norway. Contrib. Mineral. Petrol. 165, 903–930.

Heinonen, J.S., Jennings, E.S., Riley, T.R., 2015. Crystallisation temperatures of the most Mg-rich magmas of the Karoo LIP on the basis of Al-in-olivine thermometry. Chem. Geol. 411, 26–35.

Hofmann, A.W., 1988. Chemical differentiation of the Earth: the relationship between mantle, continental crust, and oceanic crust. Earth Planet. Sci. Lett. 90, 297–314.

Hollocher, K., Robinson, P., Walsh, E., Terry, M.P., 2007. The Neoproterozoic Ottfjället dike swarm of the middle Allochthon, traced geochemically into the Scandian hinterland, Western Gneiss Region, Norway. Am. J. Sci. 307, 901–953.

Jennings, E.S., Gibson, S.A., Maclennan, J., Heinonen, J.S., 2017. Deep mixing of mantle melts beneath continental flood basalt provinces: Constraints from olivine-hosted melt inclusions in primitive magmas. Geochim. Cosmochim. Acta 196, 36–57.

Jochum, K.P., Weis, U., Stoll, B., Kuzmin, D., Yang, Q., Raczek, I., Jacob, D.E., Stracke, A., Birbaum, K., Frick, D.A., Günther, D., Enzweiler, J., 2011. Determination of reference values for NIST SRM 610–617 glasses following ISO guidelines. Geostand. Geoanal. Res. 35, 397–429.

Kamenetsky, V.S., Chung, S.L., Kamenetsky, M.B., Kuzmin, D.V., 2012. Picrites from the Emeishan Large Igneous Province, SW China: a compositional continuum in primitive magmas and their respective mantle sources. J. Petrol. 53, 2095–2113.

Kent, A.J., Baker, J.A., Wiedenbeck, M., 2002. Contamination and melt aggregation processes in continental flood basalts: constraints from melt inclusions in Oligocene basalts from Yemen. Earth Planet. Sci. Lett. 202, 577–594.

Kohn, S.C., Schofield, P.F., 1994. The importance of melt composition in controlling trace-element behaviour: an experimental study of Mn and Zn partitioning between forsterite and silicate melts. Chem. Geol. 117, 73–87.

Larsen, R.B., Grant, T., Sørensen, B.E., Tegner, C., McEnroe, S., Pastore, Z., Fichler, C., Nikolaisen, E., Grannes, K.R., Church, N., ter Maat, G.W., 2018. Portrait of a giant deep-seated magmatic conduit system: The Seiland Igneous Province. Lithos 296, 600–622.

Larsen, R.B., Sørensen, B.E., Nikolaisen, E., 2019. Formation and disruption of Cu-Ni-PGE deposits in a giant deep-seated mafic-ultramafic conduit system. 15th Biennial SGA Meeting, Glasgow, UK.

Lee, C.T.A., Lee, T.C., Wu, C.T., 2014. Modelling the compositional evolution of recharging, evacuating, and fractionating (REFC) magma chambers: Implications for differentiation of arc magmas. Geochim. Cosmochim. Acta 143, 8–22.

Mørk, M.B.E., Stabel, A., 1990. Cambrian Sm—Nd dates for an ultramafic intrusion and for high-grade metamorphism on the Øksfjord peninsula, Finnmark, North Norway. Nor. Geol. Tidsskr. 70, 275–291.

Müntener, O., Ulmer, P., 2006. Experimentally derived high-pressure cumulates from hydrous arc magmas and consequences for the seismic velocity structure of lower arc crust. Geophys. Res. Lett. 33.

Nielsen, T.F.D., Turkov, V.A., Solovova, I.P., Kogarko, L.N., Ryabchikov, I.D., 2006. A Hawaiian beginning for the Iceland plume: Modelling of reconnaissance data for olivine-hosted melt inclusions in Palaeogene picrite lavas from East Greenland. Lithos 92, 83–104.

Orvik, A.A., 2019. The dyke swarm in the Reinfjord Ultramafic Complex; a window into the terminal stages forming the Seiland Igneous Province Master's thesis, NTNU.

Pastore, Z., Fichler, C., McEnroe, S.A., 2016. The deep crustal structure of the mafic–ultramafic Seiland Igneous Province of Norway from 3-D gravity modelling and geological implications. 207. Geophysical Supplements to the Monthly Notices of the Royal Astronomical Society, pp. 1653–1666.
Pedersen, R.B., Dunning, G.R., Robins, B., 1989. U—Pb ages of nepheline syenite pegmatites from the Seiland Magmatic Province, N. Norway. Caledonide Geol. Scand. 3–8.
Pertermann, M., Hirschmann, M.M., 2003. Anhydrous partial melting experiments on MORB-like eclogite: phase relations, phase compositions and mineral–melt partitioning of major elements at 2–3 GPa. J. Petrol. 44, 2173–2201.
Pertermann, M., Hirschmann, M.M., Hametner, K., Günther, D., Schmidt, M.W., 2004. Experimental determination of trace element partitioning between garnet and silica-rich liquid during anhydrous partial melting of MORB-like eclogite. Geochem. Geophys. Geosyst. 5.
Presnall, D.C., Dixon, S.A., Dixon, J.R., O'Donnell, T.H., Brenner, N.L., Schrock, R.L., Dycus, D.W., 1978. Liquidus phase relations on the join diopside-forsterite-anorthite from 1 atm to 20 kbar: their bearing on the generation and crystallisation of basaltic magma. Contrib. Mineral. Petrol. 66, 203–220.
Reginiussen, H., Ravna, E.K., Berglund, K., 1995. Mafic dykes from Øksfjord, Seiland Igneous Province, northern Norway: geochemistry and palaeotectonic significance. Geol. Mag. 132, 667–681.
Riley, T.R., Leat, P.T., Curtis, M.L., Millar, I.L., Duncan, R.A., Fazel, A., 2005. Early–Middle Jurassic dolerite dykes from Western Dronning Maud Land (Antarctica): identifying mantle sources in the Karoo large igneous province. J. Petrol. 46, 1489–1524.
Roberts, R.J., Corfu, F., Torsvik, T.H., Ashwal, L.D., Ramsay, D.M., 2006. Short-lived mafic magmatism at 560–570 Ma in the Norwegian Caledonites: U—Pb zircon ages from the Seiland Igneous Province. Geol. Mag. 143, 887–903.
Roberts, R.J., Corfu, F., Torsvik, T.H., Hetherington, C.J., Ashwal, L.D., 2010. Age of alkaline rocks in the Seiland Igneous Province, Northern Norway. J. Geol. Soc. 167, 71–81.
Robins, B., 1975. Ultramafic nodules from Seiland, northern Norway. Lithos 8, 15–27.
Robins, B., Gardner, P.M., 1975. The magmatic evolution of the Seiland Igneous Province and Caledonian plate boundaries in Northern Norway. Earth Planet. Sci. Lett. 26, 167–178.
Robins, B., Takla, M.A., 1979. Geology and geochemistry of o metamorphosed picrate-ankaramite dyke suite from the Seiland province, northern Norway. Nor. Geol. Tidsskr. 59, 67–95.
Røisi, I., 2018. Geochemistry of carbonatite and syenite samples from the Breivikbotn alkaline complex, Sørøya, Hasvik, Finnmark, Norway (Dept. of Geoscience and Petroleum Internal Report Series M-KAA 2018:4). Trondheim:Dept. of Geoscience and Petroleum, NTNU unpublished.
Sobolev, A.V., Hofmann, A.W., Kuzmin, D.V., Yaxley, G.M., Arndt, N.T., Chung, S.L., Danyushevsky, L.V., Elliott, T., Frey, F.A., Garcia, M.O., Gurenko, A.A., 2007. The amount of recycled crust in sources of mantle-derived melts. Science 316, 412–417.
Sobolev, A.V., Krivolutskaya, N.A., Kuzmin, D.V., 2009. Petrology of the parental melts and mantle sources of Siberian trap magmatism. Petrology 17, 253.
Sørensen, B.E., Grant, T., Ryan, E.J., Larsen, R.B., 2019. In situ evidence of earthquakes near the crust mantle boundary initiated by mantle CO2 fluxing and reaction-driven strain softening. Earth Planet. Sci. Lett. 524, 115,713.
Sturt, B.A., Speedyman, D.L., Griffin, W.L., 1980. The Nordre Brumandsfjord ultramafic pluton, Seiland, North Norway. Part I: field relations. Nor. Geol. Unders. 358, 1–30.
Sun, S.S., McDonough, W.F., 1989. Chemical and isotopic systematics of oceanic basalts: implications for mantle composition and processes. Geol. Soc. Lond. Spec. Publ. 42, 313–345.
Svensen, S.A., 1990. Geologi of petrologi i nordøstlige del av. Kvalfjord ultramafiske kompleks Stjernøya, Finnmark Unpublished Masters thesis, Univeristy of Bergen (unpublished).
Tappe, S., Pearson, D.G., Nowell, G., Nielsen, T., Milstead, P., Muehlenbachs, K., 2011. A fresh isotopic look at Greenland kimberlites: cratonic mantle lithosphere imprint on deep source signal. Earth Planet. Sci. Lett. 305, 235–248.
Tegner, C., Robins, B., Reginiussen, H., Grundvig, S., 1999. Assimilation of crustal xenoliths in a basaltic magma chamber: Sr and Nd isotopic constraints from the Hasvik layered intrusion, Norway. J. Petrol. 40, 363–380.
Tegner, C., Andersen, T.B., Kjøll, H.J., Brown, E.L., Hagen-Peter, G., Corfu, F., Torsvik, T.H., 2019. A mantle plume origin for the Scandinavian Dyke Complex: a "piercing point" for 615 Ma plate reconstruction of Baltica? Geochem. Geophys. Geosyst. 20, 1075–1094.
Thompson, R.N., Gibson, S.A., 2000. Transient high temperatures in mantle plume heads inferred from magnesian olivines in Phanerozoic picrites. Nature 407, 502.
Tuff, J., Takahashi, E., Gibson, S.A., 2005. Experimental constraints on the role of garnet pyroxenite in the genesis of high-Fe mantle plume derived melts. J. Petrol. 46, 2023–2058.
Workman, R.K., Hart, S.R., 2005. Major and trace element composition of the depleted MORB mantle (DMM). Earth Planet. Sci. Lett. 231, 53–72.
Wulff-Pedersen, E., 1992. Petrological and metamorphic evolution of carbonate lithologies on Øksfjordhalvøya, N. Norway (in Norwegian). (Unpubl. MSc-thesis). University of Tromsø (unpublished). p. 144.
Yaxley, G.M., Kamenetsky, V.S., Kamenetsky, M., Norman, M.D., Francis, D., 2004. Origins of compositional heterogeneity in olivine-hosted melt inclusions from the Baffin Island picrites. Contrib. Mineral. Petrol. 148, 426–442.
Yeo, W.J.A., 1984. The Melkvann Ultramafic Complex, Seiland igneous province, North Norway: intrusive mechanisms and petrological evolution Unpublished Ph.D. thesis, University of Bristol, U.K (unpublished).
Yu, X., Lee, C.T.A., Chen, L.H., Zeng, G., 2015. Magmatic recharge in continental flood basalts: Insights from the Chifeng igneous province in Inner Mongolia. Geochem. Geophys. Geosyst. 16, 2082–2096.